



Spiking dynamics of bidimensional integrate-and-fire neurons

Jonathan Touboul, Romain Brette

► To cite this version:

Jonathan Touboul, Romain Brette. Spiking dynamics of bidimensional integrate-and-fire neurons. SIAM Journal on Applied Dynamical Systems, 2009. inria-00276924v5

HAL Id: inria-00276924

<https://inria.hal.science/inria-00276924v5>

Submitted on 11 Jun 2018

HAL is a multi-disciplinary open access archive for the deposit and dissemination of scientific research documents, whether they are published or not. The documents may come from teaching and research institutions in France or abroad, or from public or private research centers.

L'archive ouverte pluridisciplinaire **HAL**, est destinée au dépôt et à la diffusion de documents scientifiques de niveau recherche, publiés ou non, émanant des établissements d'enseignement et de recherche français ou étrangers, des laboratoires publics ou privés.

SPIKING DYNAMICS OF BIDIMENSIONAL INTEGRATE-AND-FIRE NEURONS

JONATHAN TOUBOUL* AND ROMAIN BRETTE †

Abstract. Spiking neuron models are hybrid dynamical systems combining differential equations and discrete resets, which generate complex dynamics. Several two-dimensional spiking models have been recently introduced, modelling the membrane potential and an additional variable, and where spikes are defined by the divergence of the membrane potential variable to infinity. These simple models reproduce a large number of electrophysiological features displayed by real neurons, such as spike frequency adaptation and bursting. The patterns of spikes, which are the discontinuity points of the hybrid dynamical system, have been mainly studied numerically. Here we show that the spike patterns are related to orbits under a discrete map, the adaptation map, and we study its dynamics and bifurcations. Regular spiking corresponds to fixed points of the adaptation map while bursting corresponds to periodic orbits. We find that the models undergo a transition to chaos via a cascade of period adding bifurcations. Finally, we discuss the physiological relevance of our results with regard to electrophysiological classes.

Key words. neuron models, spike patterns, hybrid dynamical systems, nonlinear dynamics, bursting, chaos.

AMS subject classifications. 37C10, 37C25, 37C27, 37G15, 39A11, 37N25, 92C20, 37B10

Update note: This version updates the condition for the existence of a plateau in theorem 3.1.

1. Introduction. Finding a computationally simple and biologically realistic model of neuron has been a great endeavor in computational neuroscience, the main interest being to be able to obtain mathematically tractable models in order to understand the nature of the nerve cell activity, and computationally simple in order to be able to compare experimental recordings with large scale brain models. The class of nonlinear bidimensional spiking neuron models with adaptation defined in (3; 16; 25) seems to present the advantages of being mathematically tractable, efficiently implemented, and able to reproduce a large number of electrophysiological signatures such as bursting or regular spiking. These models emulate the membrane potential of the nerve cell v together with an adaptation variable w , and distinguishes between to phases of the neuronal activity: the *subthreshold* behavior corresponding to the input integration at the level of the cell, and the emission of action potentials (spikes). The subthreshold dynamics is governed by the following ordinary differential equation:

$$\begin{cases} \frac{dv}{dt} = F(v) - w + I \\ \frac{dw}{dt} = a(bv - w) \end{cases} \quad (1.1)$$

where a, b are real parameters accounting respectively for the time constant ratio between the adaptation variable and the membrane potential and to the coupling strength between these two variables, I is a real parameter modeling a DC-input current in the neuron, and F is a real function accounting for the leak and spike initiation currents. Following (25), we assume F to be regular (at least three times

*Odyssee Laboratory, INRIA/ENS, INRIA, Sophia-Antipolis, 2004 route des Lucioles, BP 93 06902, Sophia-Antipolis Cedex, France (jonathan.touboul@sophia.inria.fr).

† 1) Laboratoire Psychologie de la Perception, Centre National de la Recherche Scientifique and Université Paris Descartes, Paris F 75006 , 2) Département d'Etudes Cognitives, Ecole Normale Supérieure, Paris F 75005, France

continuously differentiable), strictly convex, and its derivative to have a negative limit at $-\infty$ and an infinite limit at $+\infty$. In order to ensure that the neuron will elicit spikes, we add the following assumption:

ASSUMPTION (A1). *There exists $\varepsilon > 0$ such that $F(v)$ grows faster than $v^{1+\varepsilon}$ when $v \rightarrow \infty$ (i.e. there exists $\alpha > 0$ such that $F(v)/v^{1+\varepsilon} \geq \alpha$ when $v \rightarrow +\infty$).*

We prove in (26) that the membrane potential blows up in finite time in these cases. Among these models, the *quadratic adaptive* model (16) corresponds to the case where $F(v) = v^2$, and has been recently used by Eugene Izhikevich and coworkers (17) in very large scale simulations of neural networks. The *adaptive exponential* model (3) corresponds to the case where $F(v) = e^v - v$, is based on an electrophysiological description of the sodium current responsible for the generation of action potentials following the work of (11), has the interest that its parameters can be related to electrophysiological quantities, and has been successfully fit to intracellular recordings of pyramidal cells (4; 18). The *quartic* model (25) corresponds to the case where $F(v) = v^4 + 2av$ and has the advantage of being able to reproduce all the behaviors featured by the other two and also self-sustained subthreshold oscillations which are of particular interest to model certain nerve cells.

As we proved in (26), in the case of the quadratic adaptive model (or when the function F diverges slower than v^2 when $v \rightarrow \infty$, i.e. when there exists $V_F > 0$ such that $F(v)/v^2$ is bounded for $v \geq V_F$), the adaptation variable blows up at the same time as the membrane potential. In these cases one is led to introduce a hard threshold, the cutoff value θ , which has no biophysical interpretation. A spike is emitted at the time t^* when the membrane potential v reaches a cutoff value θ , and the membrane potential is instantaneously reset to a constant value v_r and the adaptation variable is updated to $w(t^*) + d$ where $w(t^*)$ is the value of the adaptation variable at the time of the spike and $d > 0$ is the spike-triggered adaptation parameter. The spiking properties are highly sensitive to changes in this cutoff parameter, as proved in (26), and therefore constitutes a new bifurcation parameter which artificially adds complexity to the model.

In this paper, we are interested in models for which the adaptation variable does not blow up. In this case, spikes are emitted when the membrane potential blows up. Therefore we shall consider models with an F function satisfying the following assumption:

ASSUMPTION (A2). *There exists $\varepsilon > 0$ such that F grows faster than $v^{2+\varepsilon}$ when $v \rightarrow \infty$ (i.e. there exists $\alpha > 0$ such that $F(v)/v^{2+\varepsilon} \geq \alpha$ when $v \rightarrow \infty$).*

In these cases as proved in (26) (see also section 2.4), the membrane potential blows up in finite time and at this explosion time the adaptation variable will converge to a finite value. A spike is emitted at the time t^* when the membrane potential blows up. At this time, the adaptation variable converges to the value

$$w(t^{*-}) \stackrel{\text{def}}{=} \left(\lim_{t \rightarrow t^*} w(t) \right).$$

At spike time, the membrane potential is reset to a constant value v_r and the adaptation variable is incremented by a positive quantity, the spike-triggered adaptation parameter:

$$v(t) \xrightarrow[t \rightarrow t^*]{} \infty \implies \begin{cases} v(t^*) = v_r \\ w(t^*) = w(t^{*-}) + d \end{cases} \quad (1.2)$$

In these models, the reset mechanism makes the value of the adaptation variable at the time of the spike critical. Indeed, when a spike is emitted at time t^* , the new

initial condition of the system (1.1) is $(v_r, w(t^*) + d)$. Therefore, this value governs the subsequent evolution of the membrane potential, and hence the spike pattern produced.

These models are *hybrid* dynamical systems, in the sense that they are defined by both a continuous and a discrete dynamical system. This structure make these models very interesting. Indeed the addition of the reset to the bidimensional continuous dynamical systems makes possible behaviors which cannot appear in autonomous bidimensional nonlinear ordinary differential equations, such as bursting and chaos (see (3; 15; 25)). In this paper we will rigorously study from a mathematical point of view these different behaviors, in order to understand their origin and to get insights about the related parameter ranges.

To this end, we precisely study in section 2 the orbits of equation (1.1) in the phase plane (v, w) in order to characterize the value of the adaptation variable at the time of the spike. We will be particularly interested in the attraction basins of the subthreshold attractors (SA), i.e. non spiking (bounded) attractors of the models. We will also introduce an essential tool to study the spike patterns, the adaptation map Φ . We will show that the properties of this map are closely linked with the dynamical properties of the subthreshold system. Section 3 will be devoted to the case where the subthreshold system has no fixed point. In that case, the neuron will fire whatever its initial condition. Therefore the study of the iterations of the map Φ will allow us to discriminate between different modes of tonic spiking. Section 4 is devoted to the case where there exist non-spiking (subthreshold) orbits. In this case, depending on the initial condition, the system can either fire infinitely many spikes (tonic spiking) or finitely many spikes (phasic spiking). In the last section 5 we comment these results from a neurocomputational viewpoint.

2. Detailed study of the subthreshold dynamics. In order to study the spike dynamics, we first need to understand the underlying continuous dynamical system defined by the differential equations. We shall call *subthreshold orbits* the orbits that do not spike (i.e., bounded orbits for positive time). Among these orbits, we will be particularly interested in the *subthreshold attractors* (SA), which are the non spiking (bounded) attractors of the subthreshold system. Since the subthreshold system is a bidimensional continuous dynamical system, these SAs are either fixed points or limit cycles.

2.1. Subthreshold Attractors. The number and stability of fixed points were studied in (25), and this study accounts for many excitability properties of these models, as described in (27). The basic local bifurcation structure is given in figure 2.1(a). The parameter a is a scaling parameter, and as a function of b and I the set of fixed points has the following structure: let us denote $v^*(x)$ the unique solution, when it exists, of the equation $F'(v^*(x)) = x$, and by $F'_{-\infty}$ the limit of $F'(x)$ for $x \rightarrow -\infty$. This value can be either finite (but nonpositive) or equal to $-\infty$. Note that because of the strict convexity assumption, if there exists a solution, it is unique. Furthermore, $v^*(x)$ is defined for any $x \in (F'_{-\infty}, \infty)$. For x in this interval, we denote $m(x) = F(v^*(x)) - xv^*(x)$ the unique minimum of the application $t \mapsto F(t) - xt$. We have:

1. If $I > -m(b)$, the system has no fixed point.
2. If $I = -m(b)$, the system has a unique fixed point, $(v^*(b), w^*(b))$, which is nonhyperbolic. It is unstable if $b > a$. Along this curve in the parameter space (I, b) , the system undergoes a saddle-node bifurcation provided that $F''(v^*(b)) \neq 0$.

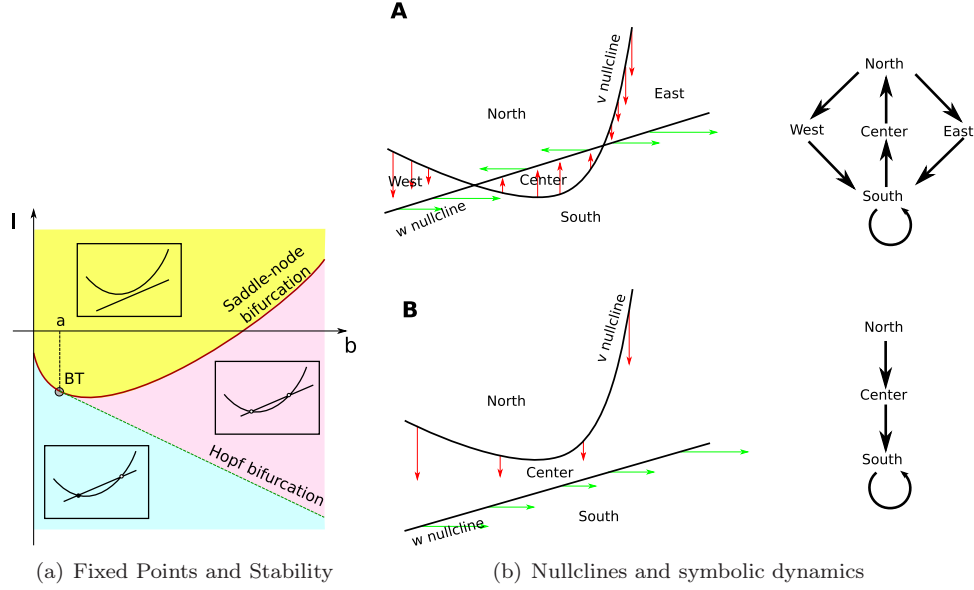


FIGURE 2.1. (a): Number of fixed points and their stability in the plane (I, b) for the exponential adaptive model. (b): Nullclines of the dynamical system (horizontal axis: v ; vertical axis: w). A. The nullclines intersect in two points, and divide the phase space into 5 regions. The potential V increases below the V -nullcline, w increases below the w -nullcline. The direction of the flow along each boundary gives the possible transitions between regions (right). Spiking can only occur in the South region. B. The nullclines do not intersect. All trajectories must enter the South region and spike.

3. If $I < -m(b)$, then the dynamical system has two fixed points $(v_-(I, b), v_+(I, b))$ such that

$$v_-(I, b) < v^*(b) < v_+(I, b).$$

The fixed point $v_+(I, b)$ is a saddle fixed point, and the stability of the fixed point $v_-(I, b)$ depends on I and on the sign of $(b - a)$:

- (a) If $b < a$, the fixed point $v_-(I, b)$ is attractive.
- (b) If $b > a$, it depends on the input current I with respect to the value $I_H(a, b) = bv^*(a) - F(v^*(a))$.
- (c) At the point $b = a$ and $I = -m(a)$, the system undergoes a Bogdanov-Takens bifurcation provided that $F''(v_a) \neq 0$. Therefore, from this point, there is a saddle homoclinic bifurcation curve characterized in the neighborhood of the Bogdanov-Takens point by

$$(P) \stackrel{\text{def}}{=} \left\{ (I, b \geq a) ; I_{Sh} = -m(a) + \frac{12}{25} \frac{(b-a)^2}{F''(v^*(a))} + o(|(b-a)^2|) \right\}. \quad (2.1)$$

- i. If $I < I_H(a, b)$, the fixed point $v_-(I, b)$ is attractive.
- ii. If $I > I_H(a, b)$, the fixed point $v_-(I, b)$ is repulsive.
- iii. On the parameter line given by

$$(AH) \stackrel{\text{def}}{=} \left\{ (b, I) ; b > a \text{ and } I = I_H(a, b) = bv^*(a) - F(v^*(a)) \right\},$$

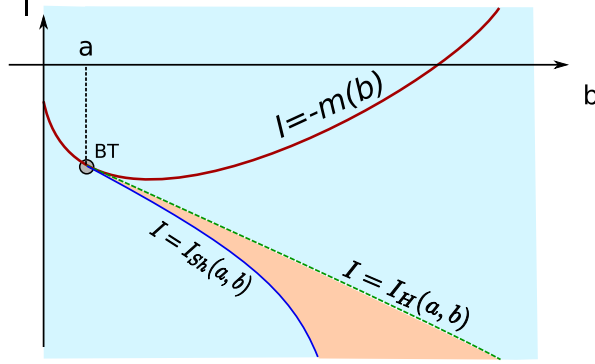


FIGURE 2.2. *Unstable limit cycles in the case where there is no Bautin bifurcation. The system has no periodic orbit in the blue zone, and a unique unstable periodic orbit in the orange zone. For a fixed $b > a$, the family appears via Hopf bifurcation at $I = I_H$ and disappears via saddle-homoclinic bifurcation at $I = I_{SH}$. BT is the Bogdanov-Takens bifurcation point.*

the system undergoes an Andronov Hopf bifurcation, whose type is given by the sign of the variable

$$A(a, b) = F'''(v^*(a)) + \frac{1}{b-a} F''(v^*(a))^2.$$

If $A(a, b) > 0$, then the bifurcation is subcritical, and if $A(a, b) < 0$, then the bifurcation is supercritical. If furthermore we have $F'''(v^*(a)) < 0$ and some technical conditions fulfilled, then the system undergoes a Bautin bifurcation at the point $v^*(a)$ for $b = a - \frac{F''(v^*(a))^2}{F'''(v^*(a))}$ and $I = bv^*(a) - F(v^*(a))$.

Let us now discuss the number and stability of periodic orbits. First of all, when the subthreshold system has no fixed point, it is clear that no limit cycle can exist, because in planar systems, the existence of a cycle implies the existence of at least one fixed point inside the cycle. In the case where the Hopf bifurcation is always subcritical the system will present unstable cycles originating from the Hopf bifurcation for $b > a$, which will collide with the saddle fixed-point manifold and disappear via saddle-homoclinic bifurcation around the Bogdanov-Takens bifurcation (see figure 2.2). For input currents between the current value corresponding to the Hopf and the saddle-homoclinic bifurcation, there exists an unstable cycle in the system. The saddle-homoclinic bifurcation curve can then be continued, and it either remains finite for all $b > a$, or tend to $-\infty$, in which case cycles would exist for any I smaller than the current associated with the Hopf bifurcation. Because of the structure of the vector field presented in figure 2.1(b).A., cycles necessarily contains the fixed point v_- , and do not include the fixed point v_+ , because the intersection of the South zone and the set $\{v \geq v_+\}$ is stable and therefore no trajectory can escape from this zone. At a subcritical Hopf bifurcation, cycles appear around the fixed point v_- , and inflate when decreasing the input current until reaching the saddle fixed point v_+ .

In the cases where the system undergoes a Bautin bifurcation, the structure of the limit cycles is slightly more complex. Indeed, in addition to the subcritical Bogdanov-Takens bifurcation, the system undergoes a Bautin bifurcation. Locally around this point, a family of stable limit cycles and family of unstable ones coexist, collide

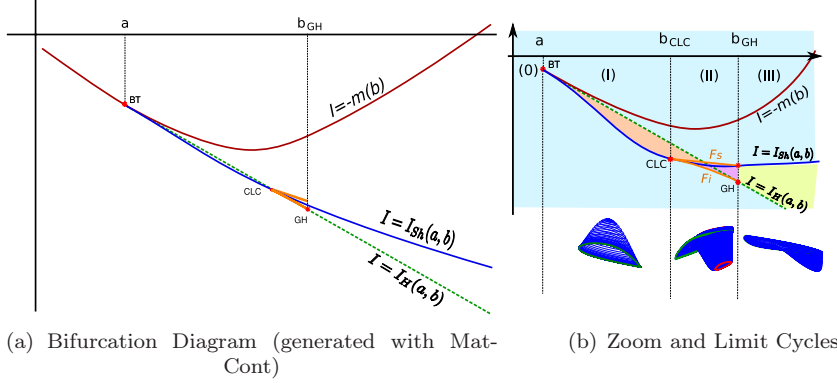


FIGURE 2.3. *Limit cycles in the case where a Bautin bifurcation exist. The saddle-node of limit cycles presents a singular point corresponding to a cusp of limit cycles. From this point emerge two branches of saddle-node of limit cycles. The lower branch of folds of limit cycles connects to the Bautin point, while the upper branch connects with the saddle-homoclinic bifurcation. (a) The orange curve represents the fold of limit cycles, the singular point CLC corresponds to a cusp of limit cycles. In the blue region there is no limit cycle. Zone (0) : No cycle. Zone (I): There exists a unique family of limit cycles in the orange zone, starting from Hopf bifurcation and disappearing via saddle-homoclinic bifurcation. Zone (II) the family of limit cycles undergoes two folds of limit cycles. There are two branches of unstable limit cycles and a branch of stable limit cycles. The family appears via subcritical Hopf bifurcation and disappears via saddle-homoclinic bifurcation. In zone (III) there is a unique family of stable limit cycles in the yellow zone for inputs between the saddle-homoclinic and the supercritical Hopf bifurcation, disappearing via saddle-homoclinic bifurcation. (b) Families of limit cycles in each case. Green cycle = saddle-homoclinic orbit, red cycle = fold of limit cycle.*

and disappear via a fold (saddle-node) bifurcation of limit cycles. We numerically computed these two curves in the case of the quartic model using the MatCont toolbox (6; 7) and present the results in figure 2.3. We observe that for $b < a$, there is no limit cycle (zone (0)).

- I. For $a < b < b_{CLC}$, there is one family of limit cycles, starting from Hopf bifurcation and disappearing via saddle-homoclinic bifurcation.
- II. For $b_{CLC} < b < b_{GH}$ the family of limit cycles undergoes two folds of limit cycles. There are two branches of unstable limit cycles and a branch of stable limit cycles. One of the branches of unstable limit cycles disappears via saddle-homoclinic bifurcation.
- III. For $b > b_{GH}$ there is a unique family of stable limit cycles in the green zone emerging from a supercritical Hopf bifurcation and disappearing via saddle-homoclinic bifurcation.

In zones (0), (I) and (III) the structure of limit cycles is quite simple. Case (II) is more complex and needs some attention (see figure 2.4). In this case, the Bautin bifurcation generates a fold of limit cycles bifurcation in its neighborhood. We observe numerically that the curve of fold of limit cycles has a singular point where the system undergoes a cusp of limit cycles. Between the Bautin bifurcation point and the cusp of limit cycles point, the curve of folds of limit cycles can be parameterized as the graph of a function of b : $\{(I, b); I = F_i(b)\}$. The second branch of fold of limit cycles branching to the first one at the cusp point disappears via saddle-homoclinic bifurcation. It can also be characterized as the graph of a function of b : $\{(I, b); I = F_s(b)\}$. For $I_H < I < F_s$ there is a unique unstable limit cycle around the stable fixed point. For $F_s < I < I_{Sh}$ there are three limit cycles, two unstable

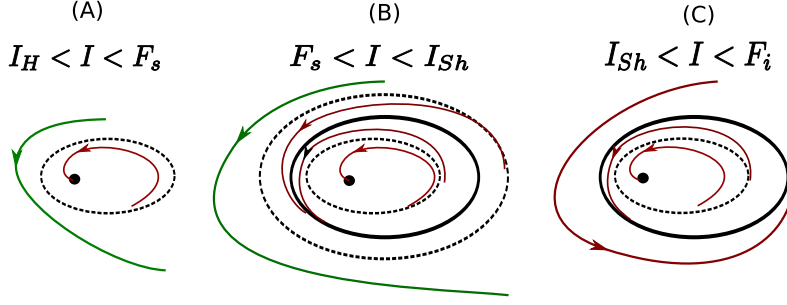


FIGURE 2.4. Families of limit cycles in zone (II) of the diagram corresponding to $b_{CLC} < b < b_{GH}$. Dashed cycles correspond to unstable periodic orbits, plain cycles to stable periodic orbit, the black dot symbolizes the fixed point. Red orbits are those attracted by the stable limit cycles or fixed point, and green orbits the other ones.

limit cycles circle a stable limit cycle. For $I_{Sh} < I < F_i$ there are two limit cycles: an unstable one around the fixed point, circled by a stable one. Therefore, in that case, the system presents self-sustained subthreshold oscillations before the Bautin bifurcation. Note eventually that zone (II) is relatively small in the parameter space.

The presence of periodic orbits shapes the structure of the stable manifold of the saddle-fixed point. We describe now the topology of this stable manifold and the shape of the attraction basins of the possible subthreshold attractors.

2.2. Stable manifold and attraction basins. We are now interested in the structure of the attraction basins of SAs. A point (v, w) belongs to the attraction basin of a SA if and only if the system (1.1) starting from this point converges towards this attractor. The topology of this set is governed by the subthreshold dynamics, and the problem of identifying in a closed form the attraction basin of the SAs is very hard to handle formally. Nevertheless in our particular case, the structure of these attraction basins can be characterized because the system has the property that the shape of this attraction basin is closely related to the structure of the stable manifold of the saddle fixed point (SMSFP).

The first order expansion of the SMSFP around the saddle fixed point is given by the eigenvalues and eigenvectors of the Jacobian matrix at this point. The SMSFP is composed of two submanifolds: one of them is locally contained in the zone $v \geq v_+$ which we denote Γ^+ and the other in the zone $v \leq v_+$ and will be denoted Γ^- . In all the cases, the submanifold Γ^+ is fully above the v -nullcline (i.e. $w \geq F(v) + I$), because of the direction of the eigenvectors of the Jacobian matrix at this point and of the shape of the vector field. This submanifold stays in the North zone described in figure 2.1(b) and this curve is the graph of an increasing function of v . The shape of the submanifold Γ^- locally in the zone $v \leq v_+$ and below the v -nullcline, depends on finer properties of the vector field, as we discuss in the sequel and in section 2.3.

2.2.1. Subcritical case:. We are first interested in the case where the system presents a unique repulsive periodic orbit. The description of the shape of the SMSFP is based on qualitative arguments including Cauchy–Lipschitz and Poincaré–Bendixon theorems. Since this orbit is a trajectory of the dynamical system, no solution can cross it because of the Cauchy-Lipschitz theorem. The attraction basin of the stable fixed point will therefore be delineated by the periodic orbit: any trajectory having its initial condition inside this closed orbit will necessarily converge to the fixed

point because of the Poincaré-Bendixon theorem, and no solution starting outside this zone can converge towards this fixed point because it cannot cross the periodic orbit. Therefore, the attraction basin of the stable fixed point is the zone in the phase plane delineated by the unstable limit cycle. In that case, the submanifold Γ^- winds around this cycle. Indeed, this submanifold can be computed using the backward equation related to (1.1). If it is an unbounded orbit, this stable manifold will split the phase plane into two zones, one of which containing the unstable limit cycle and the stable fixed point. Any trajectory starting in the zone containing the stable fixed point will either converge to the fixed point if it is inside the attraction basin of this fixed point delineated by the unstable periodic orbit, or will be trapped inside this zone and will not enter inside the periodic orbit. In the latter case, this trajectory cannot diverge because of the structure of the trajectories and the shape of Γ^+ . The Poincaré-Bendixon theorem would imply that there exists a stable fixed point or a stable periodic orbit in this zone which is not the case. Therefore the shape Γ^- will necessarily be bounded, and because of Poincaré-Bendixon's theorem, it will either converge to a fixed point or to a periodic orbit. Since there is no stable fixed point reachable by the stable manifold (the stable fixed point is repulsive for the backwards dynamics, and is trapped in the limit cycle), this orbit will converge to the limit cycle (see figure 2.5(a)).

In the cases where there is no unstable limit cycle around the SA (i.e. for $b < a$, or $b > a$ and $I < I_{Sh}$), the attraction basin of the SA will be unbounded, and its shape will be deduced from the shape of the SMSFP.

For the submanifold Γ^- , several cases can occur, depending on the limit of the derivative of F at $-\infty$, which we denote $F'_{-\infty}$.

- The stable manifold of the saddle fixed point can cross both nullclines (see figure 2.5(b)). As proved in (27), this will be the case when $F'_{-\infty} > -\infty$ and if $b \geq \frac{(F'_{-\infty} + a)^2}{4a}$,
- It can cross the w -nullcline (which will always be the case when $a < -F'_{-\infty}$) but not the v -nullcline. In this case, the SMSFP is the graph of a function of v , that will be decreasing before it crosses the nullcline and increasing after this point (see figure 2.5(d)),
- It can cross no nullcline, and in this case the separatrix is the graph of an increasing function of v (see figure 2.5(c)). This case never occurs when $F'_{-\infty} = -\infty$.

In these cases, the SMSFP is unbounded, and splits the phase plane into two connected components, one of which containing the SA. This component is the attraction basin of the SA.

Hence we conclude that the attraction basin of the stable fixed point is either bounded and delineated by the unstable limit cycle, or unbounded and delineated by the stable manifold of the saddle fixed point.

2.2.2. Bautin case. This dichotomy also applies in the case where the system undergoes a Bautin bifurcation: if the SA (fixed point or stable periodic orbit) is circled by an unstable limit cycle, then the attraction basin of the SA will be delineated by this cycle, and if not, the attraction basin will be delineated by the SMSFP.

Consider for instance the case of figures 2.3 and 2.4. Using the notations of figure 2.3 we can prove that:

- When there is no fixed point, the system has no SA and there is no saddle fixed point.

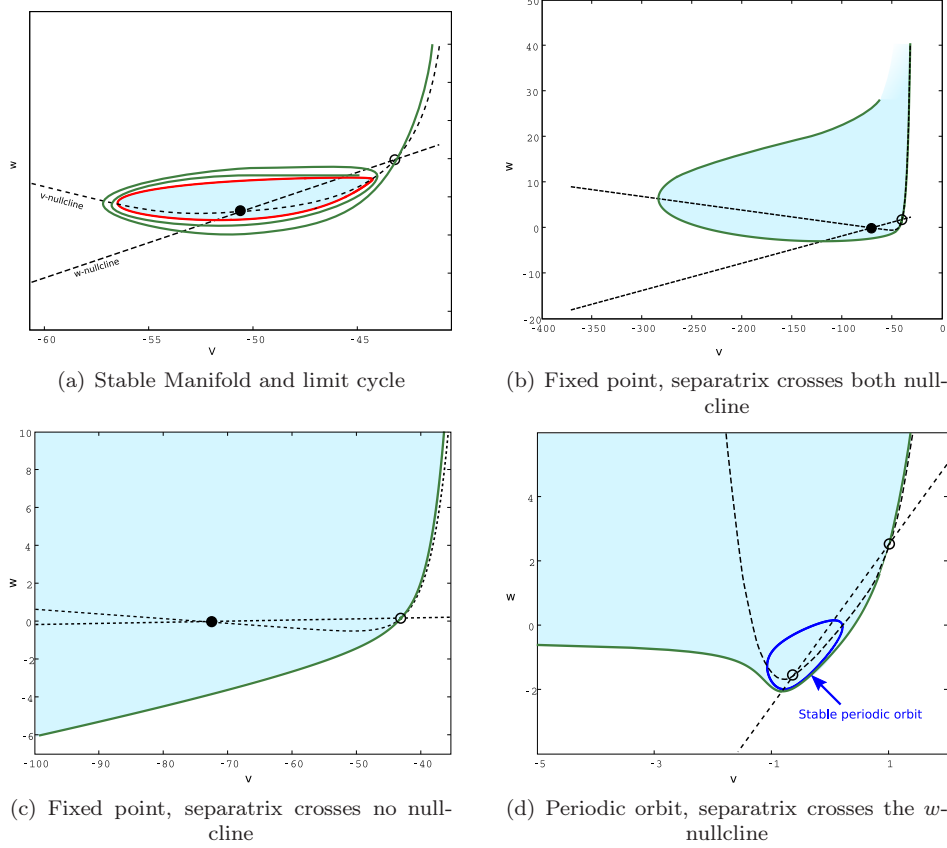


FIGURE 2.5. Representation of the attraction basin and the stable manifold of the saddle fixed point in different cases. (a): A repulsive limit cycle (red curve) exists around the stable fixed point (black circle), the SMSFP (green line) converges towards the cycle, and the attraction basin (blue zone) is bounded. The black dashed lines corresponds to the nullclines. (b): Case where the separatrix crosses both nullclines (same color code), in the case of the adaptive exponential model with original parameters except $a = 2g_L$ and $\tau_m = \tau_w$; (c): Case where the stable manifold crosses no nullcline: it is the graph of an increasing function of v which delineates the attraction basin of the stable fixed point (case of the dimensioned adaptive exponential model with the original parameters except $a = 2g_L$ and $\tau_w = \tau_m/3$); (d): Case where the stable manifold only crosses the w -nullcline. It was represented in the case where the stable trajectory is a periodic orbit (quartic model, $a = 1$, $b = 2.51 > b_{GH}$, $I = -0.5$).

- For $b < a$ and $I < -m(b)$, the system has a unique stable fixed point whose attraction basin is unbounded and delineated by the SMSFP.
- For $a < b < b_{CLC}$, the case is very similar to the subcritical case and the behavior depends on the input current:
 - If $I_H < I < -m(b)$ the system has no SA and two unstable fixed points. This case is treated in section 2.3.
 - If $I_{Sh} < I < I_H$ where I_{Sh} is the value of the current at the saddle-homoclinic bifurcation, the system has a unique SA which is a stable fixed point, circled by an unstable limit cycle. This periodic orbit delineates the attraction basin of the stable fixed point and the SMSFP winds around it

- If $I < I_{Sh}$ the system has a unique stable fixed point whose attraction basin is unbounded and delineated by the SMSFP.
- For $b_{CLC} < b < b_{GH}$, we have:
 - For $I_{SN} < I < \max(I_H, F_s)$ there are two unstable fixed points and no periodic orbit, hence no SA.
 - For $\max(I_H, F_s) < I < F_s$, the system has a unique SA which is a stable fixed point, circled by an unstable limit cycle. This periodic orbit delineates the attraction basin of the stable fixed point and the SMSFP winds around it (case of figure 2.5(a)).
 - For $F_s < I < I_{Sh}$ the system has two SAs: a fixed point and a stable limit cycle (see figure 2.4(B)). The stable fixed point is circled by an unstable limit cycle which delineates its attraction basin. The stable periodic orbit is contained in a ring delineated by two unstable limit cycles. This ring is the attraction basin of the stable limit cycle. The submanifold Γ^- of the SMSFP winds around the exterior unstable limit cycle.
 - For $I_{Sh} < I < F_i$ the system has a stable fixed point whose attraction basin is delineated by an unstable periodic orbit circling around it (see figure 2.4(C)). Around this cycle there is a stable limit cycle, whose attraction basin is an unbounded zone with one hole delineated by the unstable limit cycle and the SMSFP which is unbounded.
 - For $I < F_i$ the system has a stable fixed point whose attraction basin is unbounded and delineated by the SMSFP.
- In the case $b > b_{GH}$, we have:
 - if $I_{Sh} < I < -m(b)$ the system has no SA and two unstable fixed points.
 - if $I_H < I < I_{Sh}$ the system has two unstable fixed points and a stable periodic orbit whose attraction basin is unbounded and delineated by the SMSFP.
 - if $I < I_H$ the system has a stable fixed point with an unbounded separatrix.

2.3. Heteroclinic orbits. In the case where there are two unstable fixed points, one of which is repulsive and the other saddle, then the component Γ^+ of the SMSFP is the graph of an increasing function of v for $v \geq v_+$ and stays above the v -nullcline. The submanifold Γ^- will connect to the repulsive fixed point, for the same reasons as mentioned in the case of the presence of an unstable limit cycle. Indeed, if we consider the backward equation starting in the neighborhood of the saddle fixed point, the repulsive fixed point of the forward dynamics becomes attractive, and it is the unique bounded trajectory possible. The stable manifold when considering the backward equation will either converge to the fixed point, or will diverge, according to Poincaré-Bendixon's theorem. But assuming that it is unbounded leads to a contradiction: if it was unbounded, it would separate two zones of the phase plane (see figure 2.5), one of which containing the unstable fixed point. A trajectory having its initial condition in this zone will be trapped in it for all $t > 0$. But in this zone, the trajectory will be bounded because of the structure of the vector field, but there is neither fixed point nor stable periodic orbit. Therefore Poincaré-Bendixon's theorem leads to a contradiction, and the stable manifold necessarily connects to the repulsive fixed point. This connection can be one of two types (see figure 2.6): a monotonous connection in the case where the eigenvalues of the Jacobian matrix of the repulsive fixed point are real, and an oscillating connection when the eigenvalues have a non-

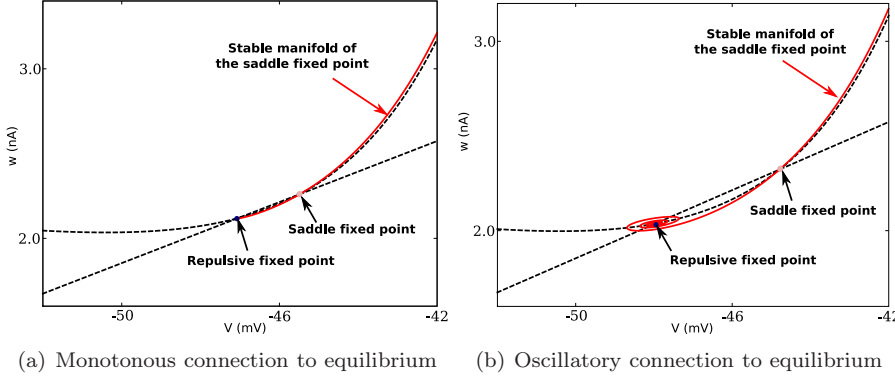


FIGURE 2.6. *Stable manifold of the saddle fixed point in the case of two unstable equilibria. Dashed black curves are the nullclines of the system and the red curve is the stable manifold.*

null imaginary part. This branch of stable manifold is therefore a heteroclinic orbit, connecting a repulsive equilibrium to a saddle equilibrium. It is structurally stable, and disappears at the Hopf bifurcation. In the case where the Hopf bifurcation is subcritical, the heteroclinic orbit connecting the repulsive fixed point and the saddle fixed point converts into a heteroclinic orbit connecting the saddle fixed point with the repulsive limit cycle and we are in the case of figure 2.5(a). In the case where the Hopf bifurcation is supercritical (after the Bautin bifurcation) the heteroclinic orbit will simply disappear. By continuity, the SMSFP will be, after the bifurcation, of type 2.5(b).

2.4. Symbolic dynamics and spiking regions. This detailed description of the subthreshold dynamics allows us to get a better insight of the dynamics and to make the diagram 2.1(b) more precise. Indeed, we are now able to provide a Markov partition of the phase plane (see fig.2.7).

- In the case $I > -m(b)$, there is no SA, and the phase plane is partitioned into the *up zone* above the v -nullcline, i.e. defined by $\{(v, w); w \geq F(v) + I\}$, the *center zone* between the two nullclines and the *spiking zone* below the w -nullcline $\{(v, w); w \leq bv\}$. We observe that any trajectory having its initial condition in the up zone enters in finite time the center zone. Indeed, while the orbit is in the up zone, the derivative of the adaptation variable is strictly inferior to $-d(F(v) + I, bv)$ the distance between the two nullclines. In the center zone, w is decreasing and v is increasing. Because of the vector field along the v -nullcline, we observe that the orbit cannot go back to the up zone. Since in this zone w is a decreasing function of v and the boundary bv an increasing function, it will enter in finite time the spiking zone. In this spiking zone defined by $w \leq bv$, the trajectory is trapped, and the membrane potential blows up in finite time.
- In the case where there are SAs, we reviewed the different shapes of the related attraction basins. These regions correspond to what we call the *rest* region, in the sense that any orbit starting inside this zone will never fire. This zone is stable under the dynamics, and does not communicate with the other zones (see figures 2.7(b), 2.7(c) and 2.7(d)). We define here again the spiking zone below both the w -nullcline and the SMSFP. This zone is also stable under the dynamics. The *right* zone is the zone above the w -nullcline and below

the SMSFP. In this zone, for any initial condition below the v -nullcline, v is increasing and w decreasing. Therefore, the derivative of v increases, and the orbit will enter the spiking zone in finite time, since the orbit is a non-increasing function of v and the boundary is strictly increasing. If the initial condition is in the right zone below the SMSFP and above the v -nullcline, both v and w will be decreasing and therefore the orbit cannot stay above the v -nullcline indefinitely, because of the presence of the unstable manifold of the saddle fixed point, and therefore will be in the right zone below the v nullcline after a finite time, and therefore in the spiking zone in finite time. The *up* zone is the rest of the phase plane. In this zone, orbits do not stay indefinitely, and cannot enter either the rest zone or the right zone, hence enter in finite time the spiking zone.

- In the cases where there are two unstable fixed points and no stable limit cycles (Figures 2.7(e) and 2.7(f)), there is no SA except from the SMSFP. We define the *up* zone above both the w -nullcline and the SMSFP, the right zone the zone between the SMSFP and the w -nullcline and the *spiking* zone below both the w -nullcline and the SMSFP. In the spiking zone, as we will see, the system will fire. For any initial condition in the right zone, since the orbit will not cross the SMSFP, it will necessarily enter the spiking zone in finite time.

This is very important in terms of spikes. Indeed, we can prove that for any initial condition in the spiking region, the membrane potential v will blow up in finite time, and therefore a spike will be emitted. Indeed, let (v_0, w_0) be a given initial condition in the bottom region at time t_0 . According to the shape of the vector field, as presented in our Markov partition, the whole trajectory will be trapped in this zone. But in this zone, we always have $w \leq v$ and therefore for all $t \geq t_0$ we have $w(t) \leq bv(t)$. According to Gronwall's theorem, the membrane potential at time $t \geq t_S$ will be greater than or equal to the solution of:

$$\begin{cases} \dot{\tilde{v}} &= F(\tilde{v}) - b\tilde{v} + I \\ \tilde{v}(t_S) &= v(t_S) \end{cases}$$

which blows up in finite time by the virtue of assumption (A1).

Therefore any trajectory entering the bottom region will spike, and furthermore any trajectory having its initial condition outside the rest region will enter the bottom region in finite time, and elicit a spike. As we have seen, the dynamics of the reset after a spike depends on the value of the adaptation variable at the times of the spikes, which we describe in the following section.

2.5. Behavior of the adaptation variable at spike times. In the spiking zone, we saw that the membrane potential blew up in finite time. This zone does not intersect the v -nullcline. Therefore, in this zone, the orbit (v, w) with initial condition (v_0, w_0) at time t_0 inside the spiking zone can be written as the graph of a function of v for all $t \geq t_0$, i.e. $w(t) = W(v(t))$ where the function W is the solution of the differential equation:

$$\begin{cases} \frac{dW}{dv} = \frac{a(bv-w)}{F(v)-w+I} \\ W(v_0) = w_0 \end{cases} \quad (2.2)$$

Proof. Let $\delta(t) = W(v(t)) - w(t)$. We have $\delta(t_0) = 0$ and furthermore, since the value of $F(v) - w + I > 0$, $\frac{d\delta}{dt} = \frac{dW}{dv} \frac{dv}{dt} - \frac{dw}{dt} = 0$, and hence $\delta(t) \equiv 0$. \square

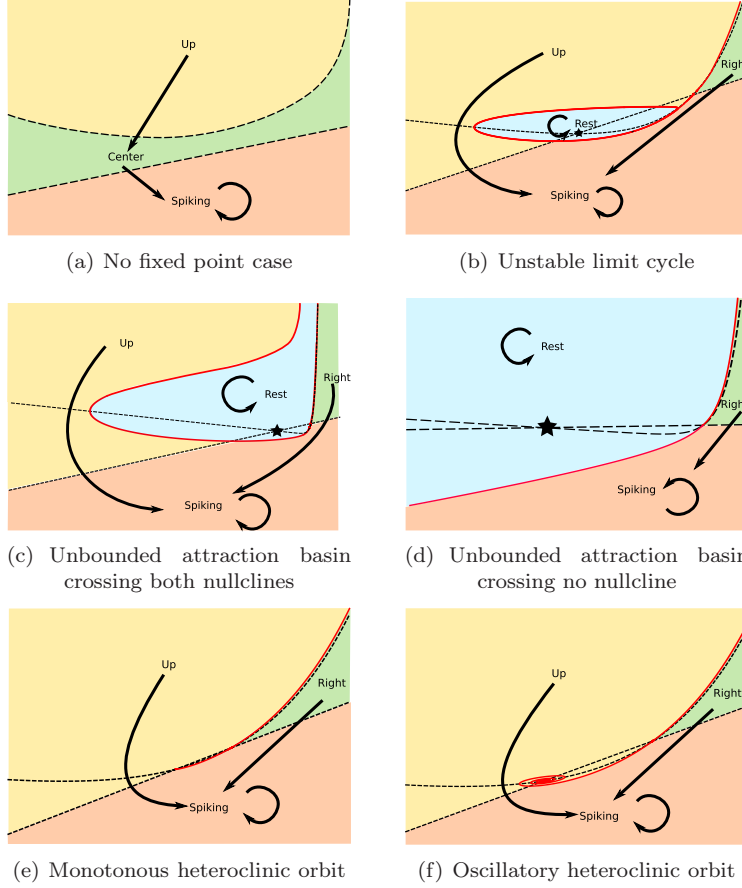


FIGURE 2.7. Markov partition of the dynamics: the bottom region is a stable region where each trajectory starting from the up or right region will end up in finite time. The rest region composed of the attraction basin of the possible stable trajectory is an isolated region.

To study the value of the adaptation variable at the explosion time of the membrane potential, we simply study the limit of the equation of the orbits when $v \rightarrow \infty$. Here we prove that this value is finite under assumption (A2), and that if $F(v)/v^2$ is asymptotically bounded, the adaptation value tends to infinity. This theorem justifies the introduction of this assumption.

THEOREM 2.1. *Under assumption (A2), the adaptation variable is finite at the times of the spikes. If $F(v)/v^2$ is bounded when $v \rightarrow \infty$, the adaptation variable at the times of the spikes tends to infinity.*

Proof. In section 2.4, we proved that all the orbits of the system that are not in the attraction basin of the (possible) stable fixed point enter after a finite time the spiking zone where they are trapped. This spiking zone is fully included in the half space $\{w < bv\}$, and in this zone the membrane potential blows up in finite time.

The value of the adaptation variable at the time of the spike can therefore be computed using the orbital equation (2.2). We consider $(v(t), w(t))$ an orbit of the differential system (1.1) such that the membrane potential blows up at time t^* . Let $(v_1 = v(t_1), w_1 = w(t_1))$ be a point of the orbit inside the spiking zone. We recall

that in the spiking zone, we have $w(t) \leq b v(t)$ and $w(t)$ is non-decreasing. Hence we have

$$\frac{dW}{dv} \leq \frac{a(bv - w_1)}{F(v) - bv + I} \quad (2.3)$$

and therefore

$$W(v) \leq w_1 + \int_{v_1}^v \frac{a(bu - w_1)}{F(u) - bu + I} du$$

If F satisfies assumption (A2), this integral converges when $v \rightarrow \infty$. Therefore, $W(v)$ (resp. $w(t)$) is an upperbounded nondecreasing function of v (resp. time), and therefore has a finite value when $v \rightarrow \infty$ (resp. $t \rightarrow t^*$).

In the case where $F(v)/v^2$ is bounded, this integral does not converge. Using the same technique, we lowerbound this value:

$$\frac{dW}{dv} \geq \frac{a(b - W)}{F(v) - w_1 + I}. \quad (2.4)$$

Gronwall's theorem (12) ensures us that the solution of equation (2.2) will be lower-bounded for $v \geq v_1$ by the solution of the linear ordinary differential equation:

$$\begin{cases} \frac{dz}{dv} = \frac{a(b-z)}{F(v)-w_1+I} \\ z(v_1) = w_1 \end{cases} \quad (2.5)$$

that reads:

$$z(v) = \left(\int_{v_1}^v \frac{a b u}{F(u) - w_1 + I} e^{-g(u)} du + w_1 \right) e^{g(v)}$$

where $g(v) = \int_{v_1}^v \frac{a du}{F(u) - w_1 + I}$. Because of assumption (A1), the integrand is integrable, and the function g has a finite limit $g(\infty)$ when $v \rightarrow \infty$. The exponential terms will hence converge when $v \rightarrow \infty$. But the integral involved in the particular solution diverges in the case where $F(v)$ grows slower than v^2 , since the integrand is equivalent when $u \rightarrow \infty$ to

$$\frac{a b u}{F(u)} e^{-g(\infty)}$$

When $F(u)$ grows slower than v^2 there exists $\alpha > 0$ such that $F(v) \leq \alpha v^2$ asymptotically and therefore the solution of the linear differential equation (2.5) tends to infinity when $v \rightarrow \infty$ faster than a logarithmic function of v , and so does $W(v)$, and hence $w(t)$ blows up at the time when $v(t)$ blows up. In the case where $F(v)$ grows slower than $v^{2-\varepsilon}$, the solution of the differential equation diverges faster than v^ε . \square

We conclude that in the case of the quadratic adaptive model, the adaptation variable blows up at the explosion time of the membrane potential variable v , and in the case of the quartic and exponential models, the adaptation variable remains bounded.

For the quadratic model, and models such that the nonlinear function $F(v)$ grows slower than a quadratic function when $v \rightarrow \infty$, the system can only be defined using

a cutoff value for the spikes. The value of the adaptation variable at the cutoff θ will be given by $W(\theta)$, and therefore will heavily depend on the cutoff value, in a very sensitive way as discussed in (26).

In the quartic and exponential models, and for any model such that $F(v)$ grows faster than $v^{2+\varepsilon}$ for a given $\varepsilon > 0$, the adaptation variable converges, and hence the model can be defined with an infinite threshold.

In these cases, for technical reasons we will use a transformed version of the orbital equation (2.2) obtained by changing variables. For (v_0, w_0) in the spiking zone, we consider $u = (v - v_0 + 1)^{-\varepsilon/2}$ where $\varepsilon > 0$ is given by assumption (A2). When $v(t)$ blows up, $u(t)$ tends to zero, and the orbit in the plane (v, u) satisfies the equation:

$$\begin{cases} \frac{d\tilde{W}}{du} = -\frac{2a(bu^{-2/\varepsilon} - \tilde{W} + \beta)}{\varepsilon u^{1+2/\varepsilon}(F(u^{-2/\varepsilon} + v_0 - 1) - \tilde{W} + I)} \stackrel{\text{def}}{=} g(u, \tilde{W}) \\ \tilde{W}(1) = w_0 \end{cases} \quad (2.6)$$

where $\beta = b(v_0 - 1)$

As we can see in equation (1.1), at the times where the membrane potential blows up and since the adaptation variable remains bounded, the derivative of the adaptation variable tends to infinity when v blows up. For this reason, accurate numerical simulations are quite hard to perform. But since in the phase plane the orbit has a regular equation, an accurate algorithm based on the simulation of the orbital equation as soon as the orbit enters the spiking zone provides a precise and stable evaluation of the adaptation value at the time of the spike using standard simulation algorithms (Runge-Kutta, Euler, ...). This method was implemented in order to produce our numerical simulations.

2.6. Existence and uniqueness of a solution. We first discuss the well-posedness of these equations. Mathematically, the problem is well-posed if the system defined by equations (1.1) and (1.2) together with an initial condition (v_0, w_0) at time t_0 has a unique solution defined for all $t \geq t_0$. The precise study we just performed gives us a better understanding of the dynamics of the subthreshold system. In particular, we saw that the solutions of the subthreshold equation (1.1) blew up in finite time, and under assumption (A2), the adaptation variable at these times has a finite value. The solutions of the subthreshold equations are hence not defined for all time. The reset condition is therefore essential to have a forward solution to the problem defined for all $t \geq t_0$. The reset condition is sufficient for the problem to be well posed, as we prove in the following:

PROPOSITION 2.2. *The equations (1.1) and (1.2), together with initial conditions (v_0, w_0) at time t_0 have a unique solution defined for $t \geq t_0$.*

Proof. Because of the regularity assumption on F , Cauchy-Lipschitz theorem of existence and uniqueness of solution applies for equation (1.1) up to the explosion time. If the solution of (1.1) does not blow up in finite time, we have existence and uniqueness of solutions for the problem. If the solution blows up at time t^* , then we are reset to a unique point, defined by the reset condition (1.2), and we are again in the case we already treated starting from $(v_r, w(t^*) + d)$ at time t^* . We can apply this mechanism again provided since the value of $w(t^*)$ is finite. Furthermore, to be able to prove the existence and uniqueness of solution for all $t \geq t_0$, we need to ensure that the interspike interval does not tend to 0 (i.e. spikes do not accumulate at a given time). The spike time decreases when the value of the adaptation on the reset line decreases. Therefore we have to ensure that the adaptation value at the times of the spike do not tend to $-\infty$. But for w_0 in the spiking zone, the value of

the adaptation variable is increasing all along the trajectory and therefore the new adaptation value after a spike is emitted will be greater than the former value plus d , and hence it is impossible that this reset value tends to $-\infty$. We conclude that the interspike interval has a lower bound on this trajectory, and between two spike times, there is a unique solution. Therefore we have existence and uniqueness of a solution starting from (v_0, w_0) which is defined for all $t \geq t_0$. \square

Another interesting question from the mathematical and neural coding points of view would be to solve the related Cauchy problem. This problem consists in proving that there exists a unique solution defined for all $t \in \mathbb{R}$. The Cauchy problem was addressed by Romain Brette in (2) in the case of spiking models defined by a one dimensional ODE with a finite spiking threshold and a reset condition. He found that the reset introduced a countable and ordered set of backward solutions for a given initial condition, and that this structure of solutions had important implications in terms of neural coding. The case of the system given by (1.1) and (1.2) can be treated in the same fashion as done in (2) and one obtains the same results as Brette in (2).

2.7. The adaptation map. Now that we are ensured that there exists a unique solution to the forward problem given by equations (1.1) and (1.2), we are interested in characterizing the spike patterns fired by a neuron of this type. These patterns are governed by the initial condition of the system after each spike, and this is why we now introduce an essential element of our work, a discrete map called the adaptation map.

DEFINITION 2.3 (The adaptation map). *We denote by \mathcal{D} the domain of adaptation values w_0 such that the solution of (1.1) with initial condition (v_r, w_0) blows up in finite time. Let $w_0 \in \mathcal{D}$, and denote $(v(t), w(t))$ the solution of (1.1) with initial condition (v_r, w_0) and t^* the blowing time of v . The adaptation map Φ is the unique function such that*

$$\Phi(w_0) = w(t^*) + d$$

The adaptation map gives the next reset location of a spiking orbit with initial condition on the *reset line* $v = v_r$. If we are interested in the spike patterns generated from an initial condition (v_0, w_0) where $v_0 \neq v_r$, the analysis will be valid after the first spike is emitted. More precisely, if (v_0, w_0) is in the attraction basin of a bounded trajectory or on the stable manifold of the saddle fixed point, then it will not elicit a spike. If it is not, then it will fire in finite time and be reset on the line $v = v_r$ at a given value w_1 . From this point, the study of the iterations of the map Φ will be valid.

Moreover, assume that in the dynamical system defined by (1.1) starting from the initial condition (v_r, w_0) is in a tonic spiking behavior (i.e. fires infinitely many spikes). Then let $(t_n)_{n \geq 0}$ be the sequence of spike times, and define the sequence of adaptation reset points by $w_n \stackrel{\text{def}}{=} w(t_n) = w(t_n^-) + d$. The adaptation map of this dynamical system is the function Φ such that

$$\Phi(w_n) = w_{n+1}$$

Hence we will be able to apply techniques of nonlinear analysis of iterations of maps to study the spiking location sequences and the spiking times.

For these reasons, we will be interested in the sequel in the dynamics of the iterations of the map Φ which corresponds to a trajectory starting from an initial

condition on the reset line. The intersections of the nullclines with the reset lines are of particular interest in the study of Φ . We define:

$$\begin{cases} w^* &= F(v_r) + I \\ w^{**} &= bv_r \end{cases} \quad (2.7)$$

Both points depend on the reset voltage v_r . Interestingly enough, besides v_r , the point w^* only depends on the input current and the nonlinearity, while the point w^{**} only depends on the parameter b . The figure Fig.2.8 represents bundles of trajectories for $w_0 < w^*$ or $w_0 > w^*$ in the case where the nullclines do not intersect. It illustrates the qualitative distinctions linked with the relative location of w with respect to w^* .

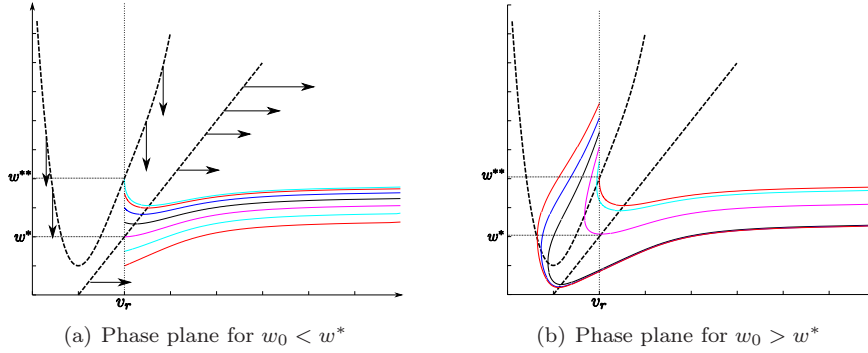


FIGURE 2.8. Phase plane and trajectories for the quartic model in the no-fixed point case. The trajectories starting from $w < w^{**}$ have an increasing w all along the trajectory, which is not the case for $w > w^{**}$. For $w > w^*$, we observe that the trajectory turns around the point (v_r, w^*) and crosses again the line $v = v_r$ before spiking.

The sequence of interspike intervals is the image of the orbit under Φ by the application $\mathcal{T} : w \in \mathcal{D} \mapsto t^*(w)$, where $t^*(w)$ is the spike time if the membrane potential starts at (v_r, w) at time $t = 0$. Although this map is not always injective, the spike patterns are qualitatively governed by the adaptation map.

Now that we introduced the main framework of our study, we will study more precisely the properties of the adaptation map Φ and its links with the spike patterns produced. The different spike patterns are linked with the topology of the domain \mathcal{D} and with properties of the map Φ . We chose here to present our results in function of the subthreshold dynamical properties, since it will make our mathematical analysis clearer. We will summarize the different regions of parameters for which a given spike pattern is produced in section 5.2.

3. No fixed point case. In this section we consider the case where there is no fixed point in for the subthreshold dynamical system. This case corresponds to the case where $I > -m(b)$ according to (25). In that case the system has neither stable fixed point nor limit cycle, and hence no bounded trajectory, and the neuron will fire whatever its initial condition, which means that the definition domain \mathcal{D} of the adaptation map Φ is \mathbb{R} .

3.1. Description of the adaptation map. We prove the following theorem.

THEOREM 3.1. *In the case $I > -m(b)$ and under the condition (A2), the adaptation map satisfies the following properties (see figure Fig.3.1):*

- It is increasing on $(-\infty, w^*]$ and decreasing on $[w^*, \infty)$,

- For all $w < w^{**}$ we have $\Phi(w) \geq w + d$,
- Φ is regular (at least continuously differentiable),
- It is concave for $w < w^*$,
- It has a unique fixed point in \mathbb{R} ,
- If $\lim_{v \rightarrow -\infty} F'(v) < -2\sqrt{ab} - a$, it has a horizontal asymptote (plateau) when $w \rightarrow +\infty$.

Update note: The original version of the paper did not include the proper condition for the existence of the plateau.

This theorem is important to understand the main properties of the *adaptation sequence* $(w_n)_{n \geq 0}$ starting from a given initial condition $w_0 \in \mathcal{D}$ defined by:

$$w_{n+1} = \Phi(w_n) \quad n \geq 0 \quad (3.1)$$

These properties would be straightforward if we had a spiking threshold, the only technical intricacy is the fact that the spike occurs when the membrane potential blows up.

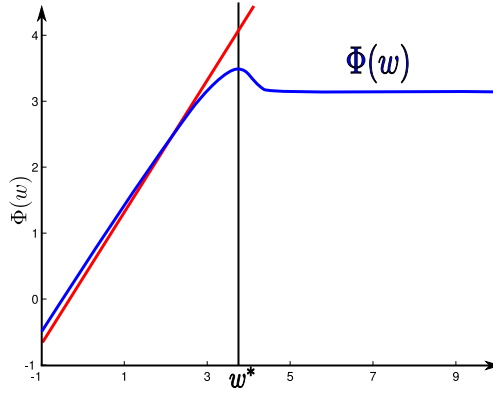


FIGURE 3.1. The adaptation map Φ in the case of the quartic model for $I > -m(b)$ (no-fixed point). The blue line corresponds to the map Φ , the red line to the identity map and the black line localizes w^* . We represent on this diagram the main properties of Φ stated in theorem 3.1 (w^{**} is smaller than -1 in this case and does not appear in this plot.)

Proof. The proof of this theorem is mainly based on a characterization of the orbits in the phase plane, given by equations (2.2) and (2.6). Using these equations, the orbit of the system with initial condition (v_r, w_0) in the spiking zone (i.e. $w_0 \leq w^*$) can be written as:

$$\tilde{W}(u; w_0) = w_0 - \int_u^1 g(s, \tilde{W}(s, w_0)) ds. \quad (3.2)$$

We have in particular

$$\Phi(w_0) = \lim_{u \rightarrow 0} \tilde{W}(u, w_0) + d. \quad (3.3)$$

- *Monotony:* Let $w_1(0) < w_2(0) \leq w^*$. The orbits $(v_1(t), w_1(t))$ having initial condition $(v_r, w_1(0))$ at time $t = 0$ and $(v_2(t), w_2(t))$ having initial condition $(v_r, w_2(0))$ at time $t = 0$ will never cross because of Cauchy-Lipschitz theorem. Since they both are in the center or in the spiking zone of diagram 2.7(a),

they satisfy equation (2.2) and since they do not cross, we will always have $\tilde{W}_1(v) \leq \tilde{W}_2(v)$, and thus $\Phi(w_1(0)) \leq \Phi(w_2(0))$.

Let us now assume that $w^* \leq w_1(0) < w_2(0)$. In that case, the initial condition is in the up zone of diagram 2.7(a). In this zone, we have seen that both variables v and w decrease. The orbit enters in finite time the center zone where v increases and w keeps decreasing. The orbits will therefore cross one time the reset line before spiking. This reset line is a Jordan section, and Jordan's theorem (see for instance (8, Chap. 9, appendix, p. 246)) implies that the solutions are always ordered on this section, and the order of the adaptation value at the two new crossing positions w_1^1 and w_2^1 is inverted, i.e. $w_2^1 < w_1^1$. By application of the previous case, we obtain

$$\Phi(w_1(0)) = \Phi(w_1^1) \geq \Phi(w_2^1) = \Phi(w_2(0)).$$

We conclude that the map Φ is increasing on $(-\infty, w^*]$ and decreasing on $[w^*, \infty)$.

- *Behavior for $w < w^{**}$* : If $w < w^{**}$, then w will increase all along the trajectory, and hence for all t smaller than the spike time t_s , we have $w(t) \geq w$ and therefore $w(t_s) \geq w$ and hence $\Phi(w) \geq w + d$.
- *Regularity*: The regularity of Φ for $w < w^*$ comes from the theorem of regularity of the solution of an ordinary differential equation with respect to its initial condition. Since in the region $w < w^*$ (center and spiking regions of diagram 2.7(a)) the value of $F(v) - w + I$ never vanishes, the orbit starting from the initial condition (v_r, w_0) satisfies equations (2.2) in the plane (v, w) and equation (2.6) in the plane (u, w) . In order to apply the regularity theorem with respect to the initial condition, we consider here equation (2.6) and check the regularity conditions.

The function g is C^∞ with respect to its two variables on $(0, 1] \times \mathbb{R}$. We prove that it is regular at the point $u = 0$. First, the map g tends to 0 when $u \rightarrow 0$ because of condition (A2), since it is equivalent when $u \rightarrow 0$ to $-2ab/(\varepsilon u^{1+4/\varepsilon} F(u^{-2/\varepsilon} + v_r - 1))$ which tends to 0 ($F(u^{-2/\varepsilon} + v_r - 1) \leq \alpha u^{-4/\varepsilon - 2}$). Furthermore it is Lipschitz on $[0, 1]$ with respect to \tilde{W} since the partial derivative of this function reads:

$$\frac{\partial g}{\partial \tilde{W}} = \frac{2a}{\varepsilon u^{1+2/\varepsilon}} \frac{(F(u^{-2/\varepsilon} + v_r - 1) - b(u^{-2/\varepsilon} + v_r - 1) + I)}{(F(u^{-2/\varepsilon} + v_r - 1) - \tilde{W} + I)^2}$$

This derivative is therefore positive, and because of assumption (A2) tends to zero when $u \rightarrow 0^+$. Therefore, this function can be extended as a continuously differentiable function in the neighborhood of 0 and using the theorem of Cauchy-Lipschitz with parameters, we conclude that the map \tilde{W} is continuous with respect to the initial condition.

We can obtain even more regularity, provided that we prove that the map g has limits for its partial derivatives of higher order. The higher order partial derivatives of g with respect to \tilde{W} will converge to zero when $u \rightarrow 0^+$ using the same argument, and by induction, we can prove that this is true for all the derivatives with respect to \tilde{W} at $u = 0^+$. The partial derivative with respect to u are slightly more intricate in the general case, but in the case of the quartic and exponential model, we can readily prove that g is C^∞ in (u, \tilde{W}) and therefore the theorem of Cauchy-Lipschitz with parameters implies that the map $\tilde{W}(\cdot, \cdot)$ and $\Phi(\cdot)$ are C^∞ .

For $w \geq w^*$, the orbit will turn around the point (v_r, w^*) . Hence Φ is the composition of the application giving the first crossing location of the orbit with the curve $\{v = v_r\}$ and Φ for $w < w^*$. The second is continuously differentiable or even more regular because of the latter argument, and the first one is C^∞ because of the standard theory of Poincaré applications (Cauchy-Lipschitz theorem with parameters for the system 1.1).

- *Concavity:* As already stated, for $w < w^*$, the solution of equation (1.1) will never cross the v nullcline, and the equation of the orbits in the phase plane (u, \tilde{W}) is given by equation (2.6), whose solution can be formally written using equation (3.2). We have:

$$\begin{cases} \frac{\partial g}{\partial \tilde{W}} &= \frac{2a}{\varepsilon u^{1+2/\varepsilon}} \frac{F(u^{-2/\varepsilon} + v_r - 1) - b(u^{-2/\varepsilon} + v_r - 1) + I}{(F(u^{-2/\varepsilon} + v_r - 1) - \tilde{W} + I)^2} > 0 \\ \frac{\partial^2 g}{\partial \tilde{W}^2} &= \frac{4ab}{\varepsilon u^{1+2/\varepsilon}} \frac{F(u^{-2/\varepsilon} + v_r - 1) - b(u^{-2/\varepsilon} + v_r - 1) + I}{(F(u^{-2/\varepsilon} + v_r - 1) - \tilde{W} + I)^3} > 0 \end{cases} \quad (3.4)$$

using the fact that $F(v) - w + I > 0$ and $w < bv$. Because of (2.6) the following formula for the second derivative of Φ with respect to w_0 .

$$\frac{\partial^2 \tilde{W}}{\partial w_0^2} = - \int_u^1 \frac{\partial^2 g}{\partial \tilde{W}^2} \left(\frac{\partial \tilde{W}}{\partial w_0} \right)^2 + \frac{\partial g}{\partial \tilde{W}} \frac{\partial^2 \tilde{W}}{\partial w_0^2},$$

Because of the second inequality (3.4) we have $\frac{\partial^2 \tilde{W}}{\partial w_0^2} \leq - \int_u^1 \frac{\partial g}{\partial \tilde{W}} \frac{\partial^2 \tilde{W}}{\partial w_0^2}$, and furthermore $\frac{\partial^2 \tilde{W}}{\partial w_0^2}(1, w_0) = 0$. Thus using Gronwall's theorem we obtain the convexity of the function $\tilde{W}(u, \cdot)$ for all u .

The adaptation map Φ is defined by

$$\Phi(\cdot) = \lim_{u \rightarrow 0} \tilde{W}(u, \cdot) + d$$

Since g is at least C^2 in the second variable, so is the flow (Cauchy-Lipschitz theorem with parameters) and hence Φ has the same convexity property for $w < w^*$.

- *Existence and uniqueness of fixed point:* Since $\Phi(w) \geq w + d$ for all $w < w^{**}$ and $\Phi(w)$ is a non-increasing function for $w > w^*$, we have existence of at least one fixed point. If $\Phi(w^*) < w^*$, then there exists a fixed point $w_{fp} \leq w^*$. Because of the concavity property of Φ , there is no other fixed point in $(-\infty, w^*)$, and since Φ is decreasing on (w^*, ∞) , it has no fixed point for $w > w^*$. If $\Phi(w^*) > w^*$, the map Φ has no fixed point for $w \leq w^*$ because of the concavity of Φ and has a unique fixed point for $w > w^*$ since Φ is non-increasing for $w > w^*$.
- *Horizontal asymptote (plateau) :* The principle of the proof is to show that there exists a solution whose membrane potential diverges to $-\infty$ when integrating the backward equation (i.e. changing t by $-t$), so that the solution separates the phase plane into two subdomains, and the orbits are trapped in one of the two domains. In the zone above this solution, the map Φ will be decreasing and lowerbounded, hence will converge when $w \rightarrow +\infty$. To prove the existence of such a solution, we search for an invariant subspace of the phase plane for the backwards dynamics (i.e for the dynamical system $(v_b(t) = v(-t), w_b(t) = w(-t))$) below the v -nullcline \mathcal{N} (i.e. included in the center or spiking zones).

It is sufficient to consider domains bounded by two lines, of type:

$$\mathcal{B} \stackrel{\text{def}}{=} \{(v, w) \mid v \leq v_0, w \leq w_0 + \alpha(v - v_0)\}$$

where the real parameters α, v_0, w_0 are free.

We show that we can find real parameters (v_0, w_0, α) such that this domain is invariant by the backwards dynamics and does not cross \mathcal{N} . We will search for non positive values of α .

First of all, for the boundary $\{v = v_0, w \leq w_0\}$, we want $\frac{dw}{dt} \leq 0$, which only means $w_b \leq w^*(v_0) = F(v_0) + I$.

Now we have to characterize both v_0 , w_0 and α such that the vector field is flowing out of the affine boundary \mathcal{B} . This means that $\langle \begin{pmatrix} \dot{v} \\ \dot{w} \end{pmatrix} | \begin{pmatrix} \alpha \\ -1 \end{pmatrix} \rangle \leq 0$ where $\langle \cdot | \cdot \rangle$ denotes the Euclidean dot product. This condition simply reads $\alpha \dot{v} - \dot{w} \leq 0$ and has to be fulfilled on each point of the boundary, which is equivalent to:

$$\begin{cases} H_\alpha(v) & \stackrel{\text{def}}{=} \alpha(F(v) - w + I) - a(bv - w) \leq 0 \text{ with} \\ w & = w_0 + \alpha(v - v_0) \end{cases} \quad (3.5)$$

We first fix α and v_0 so that \mathcal{B} is fully included in the center or spiking zones. This condition is achieved by taking $v_0 < v^*(0)$, the value where F achieves its minimum, and $\lim_{v \rightarrow -\infty} F'(v) < \alpha < F'(v_0) < 0$. Because of the convexity assumption on F , we have for all $v < v_0$, $F(v) > F(v_0) - \xi(v - v_0)$, with $\xi = -F'(v_0) > 0$ for v_0 strictly smaller than the value associated with the minimum of F . Let us now choose α such that

$$\lim_{v \rightarrow -\infty} F'(v) < -\xi = F'(v_0) < \alpha < 0.$$

We have on the boundary of the domain and for $v < v_0$:

$$\begin{aligned} H_\alpha(v) &\leq \alpha(F(v_0) - \xi(v - v_0) - w_0 - \alpha(v - v_0) + I) - a(bv - w_0 - \alpha(v - v_0)) \\ &\leq |v - v_0|(\alpha^2 + \alpha(\xi - a) + ab) + H_\alpha(v_0) \end{aligned}$$

It is easy to find w_0 small enough such that for any α satisfying our condition, $H_\alpha(v_0) < 0$. A sufficient condition on α for $H_\alpha(v)$ to be negative for all $v < v_0$ is thus:

$$\alpha^2 + \alpha(\xi - a) + ab < 0$$

Because this polynomial has a positive leading coefficient, finding an $\alpha < 0$ satisfying this condition requires (1) that the polynomial has two roots, and (2) that α falls between those roots, i.e. at least one of the roots is strictly negative. This provides the condition on $\lim_{v \rightarrow -\infty} F'(v)$. Indeed, for these conditions to apply, we need that:

I. The discriminant of the quadratic equation shall be strictly positive:

$$(\xi - a)^2 > 4ab,$$

i.e. either (i) $\xi > a + 2\sqrt{ab}$ or (ii) $0 < \xi < a - 2\sqrt{ab}$.

II. at least one of the roots is strictly negative, i.e.:

$$-(\xi - a) - \sqrt{(\xi - a)^2 - 4ab} < 0$$

In case (i), since $\xi - a > 0$, the above inequality is readily satisfied. In case (ii), the first term is positive, and we thus need:

$$0 < (a - \xi) < \sqrt{(\xi - a)^2 - 4ab}$$

which is never satisfied because $ab > 0$.

Let us thus fix v_0 such that $F'(v_0) < -a - 2\sqrt{ab}$ and α arbitrary in the interval $(F'(v_0), 0)$. The constant term $H_\alpha(v_0)$ reads:

$$(a - \alpha)w_0 + \alpha I + \alpha F(v_0) - abv_0$$

and hence involves a term proportional to w_0 with a positive coefficient, and w_0 is the last free parameter of the boundary. Choosing a sufficiently small value of w_0 ensures $H_\alpha(v_0) < 0$.

We have defined a domain \mathcal{B} on the boundary of which the vector field flows outwards, and hence the backward equation's vector field flows inwards this zone. Therefore, \mathcal{B} is flow invariant for the backward solution, and every solution having its initial condition in this zone does not cross the nullcline, hence goes to infinity with a speed lowerbounded by the minimal distance between the nullcline and \mathcal{B} .

We have proved that there is an orbit such that the membrane potential of the backward solution goes to $-\infty$, and whose forward solution spikes (since the initial condition is in the spiking zone). This solution necessarily crosses the line $\{v = v_r\}$; denote w_L the value of w at this intersection. This solution splits the phase space in two subspaces which do not communicate: every orbit starting in one of the two subspaces will stay in this subspace by application of Cauchy-Lipschitz theorem. Hence for all $w > w^*$, $\Phi(w) \geq \Phi(w_L)$, hence Φ is decreasing and lowerbounded, hence converges to a finite value when $w \rightarrow +\infty$ and its graph presents an horizontal asymptote.

□

We characterized the shape of the adaptation map in the case where the sub-threshold system has no fixed point. In this case, the spiking will necessarily be of *tonic* type, i.e. the neuron will fire infinitely many spikes (this will be the case whenever $\Phi(\mathcal{D}) \subset \mathcal{D}$). Since the system has a tonic spiking behavior, the study of the adaptation sequence of iterations of Φ provides a good way to understand the different tonic spiking patterns observed in these models.

3.2. Regular spiking. As observed numerically in (25) and as we can see in figure 3.2, the regular spiking is linked with the presence in the hybrid system of a generalized limit cycle, the *regular spiking limit cycle*, virtually containing one point having an infinite value of the membrane potential. From a mathematical point of view, this property simply corresponds to the convergence of the adaptation sequence (3.1). Indeed, if this sequence converges, then the frequency of the spikes will also converge¹.

¹If the adaptation sequence does not converge, the only way for the neuron to fire spikes regularly corresponds to the case where the sequence jumps between points corresponding to the same spike time. This occurs when the ISI map \mathcal{T} is not one-to-one. In that particular case, there is necessarily a point lower than w^* which corresponds to a sharp after-potential and the a point greater than w^* corresponding to a broad after potential, and the sequence will then be considered as a regular bursting from a biophysical point of view as well as from our mathematical point of view.

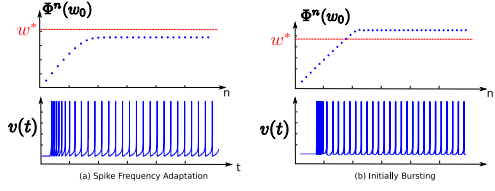


FIGURE 3.2. *Spiking generalized limit cycle, case of the quartic model. In the simulation, we have cut the trajectories to a given threshold. Threshold has been taken large enough to ensure we simulate the intrinsic system. Green dotted curves represent the nullclines, the red circles the sequence of reset positions, the solid black curves the orbit of the solution of the differential equation and the dotted lines the reset.*

Since we do not have closed form expressions for the map Φ , we provide here sufficient conditions on the dynamics of Φ leading to a regular spiking behavior.

THEOREM 3.2. *Assume that $\Phi(w^*) \leq w^*$. Then the adaptation sequence (3.1) converges for any initial condition.*

Proof. First of all we note that the interval $(-\infty, w^*]$ is stable under Φ . Indeed, Φ is increasing on this interval, therefore for all $w \in (-\infty, w^*]$, $\Phi(w) \leq \Phi(w^*) \leq w^*$. Similarly, we necessarily have $w^{**} < w^*$, since theorem 3.1 ensures us that for all $w < w^{**}$ we have $\Phi(w) > w$, and the interval $[w^{**}, w^*]$ is invariant under Φ since $w^{**} \leq \Phi(w^{**}) \leq \Phi(w^*) \leq w^*$. Therefore, the fixed point of Φ is contained in this interval.

Moreover Φ maps the interval $[w^*, \infty)$ on the interval $(-\infty, \Phi(w^*)]$ since Φ is decreasing on this interval, and therefore for all $w \in [w^*, \infty)$, we have $\Phi(w) \leq \Phi(w^*) \leq w^*$. Therefore, it is sufficient to prove that the sequence of iterates of Φ converges on $(-\infty, w^*]$.

For $w_0 \in [w^{**}, w^*]$, the sequence $(w_n)_{n \geq 0}$ is a monotonous sequence (since Φ is increasing on this interval) in a compact set, and hence will necessarily converge to the unique fixed point of Φ .

If $w_0 < w^{**}$ then $\Phi(w_n) \geq w_n + d$ while $w_n \leq w^{**}$ and hence there exists an index N such that $w^{**} \leq w_N \leq w^*$, and the previous result applies and gives us the convergence of the sequence.

We conclude therefore that for any initial condition $w \leq w^*$ the sequence converges to the unique fixed point of Φ , and since Φ maps the interval $[w^*, \infty)$ on $(-\infty, w^*]$, for any initial condition in this interval, the sequence (3.1) will converge to the fixed point of Φ . \square

The following theorem provides a sufficient condition on the map Φ to get regular spiking or bursts of period two.

THEOREM 3.3. *Assume that $\Phi(w^*) \geq w^*$ and $\Phi^2(w^*) \geq w^*$. Then the adaptation sequence either converges to the fixed point of Φ or to a period two cycle.*

Proof. Let w_0 be a given initial condition for the sequence (3.1). Necessarily this sequence (w_n) will enter the interval $[w^*, \Phi(w^*)]$ after a finite number of iterations. Indeed, assume that $w_0 < w^*$. Since there is no fixed point in $(-\infty, w^*)$, Φ is increasing and $\Phi(w) \geq w$ in this interval, the sequence cannot be upperbounded by w^* . Hence there will be an integer p such that $\Phi^p(w_0) \leq w^*$ and $\Phi^{p+1}(w_0) \geq w^*$. Then because of the monotony of Φ on $(-\infty, w^*)$ we have $\Phi^{p+1}(w_0) \leq \Phi(w^*)$. Thus $w_{p+1} \in [w^*, \Phi(w^*)]$. If $w_0 > w^*$, because of the monotony of Φ on (w^*, ∞) we have $\Phi(w_0) \leq \Phi(w^*)$ and hence the sequence will enter the interval $[w^*, \Phi(w^*)]$ after a finite number of iterations.

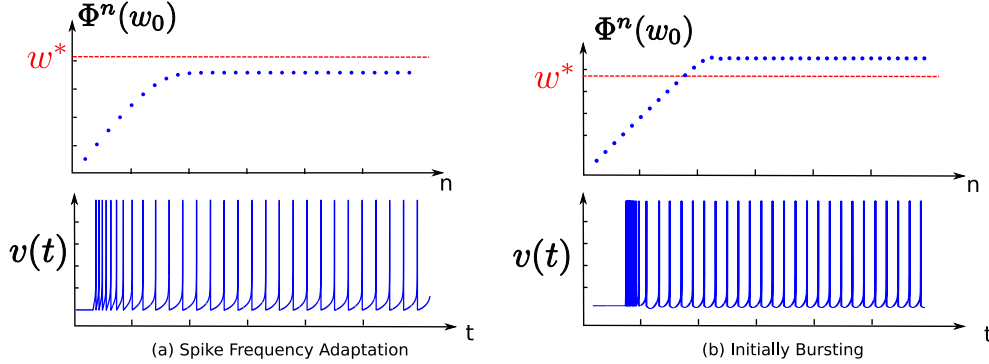


FIGURE 3.3. *Regular spiking. The different transient phases (initially bursting, spike frequency adaptation) are linked with the relative position of the fixed point with respect to w^* .*

Moreover, the interval $[w^*, \Phi(w^*)]$ is stable under Φ , since Φ is decreasing on this interval, and

$$\Phi([w^*, \Phi(w^*)]) = [\Phi^2(w^*), \Phi(w^*)] \subset [w^*, \Phi(w^*)].$$

Let $w \in [w^*, \Phi(w^*)]$ and $w_n = \Phi^n(w)$ the related adaptation sequence. Since Φ^2 is increasing on this invariant bounded interval, the sequences (w_{2n}) and (w_{2n+1}) are monotonous and both converge to a fixed point of Φ^2 , hence (w_n) either converges to a fixed point of Φ or to a periodic orbit of period two depending on the stability of the fixed point. \square

We have identified two simple sufficient conditions on Φ to obtain a regular spiking behavior. These criteria are not directly related to the parameters of the model, but they will be useful in order to describe mathematically the dependency with respect to the parameters as done in section 3.4. They can also be used in numerical simulations to compute the zones of parameters corresponding to this regular spiking behavior, as we do in section 5.2.

This analysis accounts for the stationary spiking behavior as well as for the transient phase, i.e. before the convergence of the sequence. In the spike patterns analysis, we generally distinguish between two types of regular spiking: the spike frequency adaptation that corresponds to the case where the spike frequency smoothly converges to its stationary value, and initial bursting mode (or mixed mode) where the neuron transiently fires a burst before spiking regularly. From the biological point of view, the distinction between these behaviors is not so clear, and we can continuously go from one behavior to the other. Mathematically, the difference between these two behaviors corresponds to the value of the fixed point of the adaptation map. Indeed, assume that the fixed point of the map Φ is smaller than w^* . In this case, when the sequence will converge towards the fixed point, the value of the adaptation sequence will always be smaller than w^* , and the orbit will present a sharp after potential. The interspike interval in this zone is quite smooth and therefore the convergence towards the fixed point will result in the smooth adaptation of the spike frequency. If the fixed point is greater than w^* , when we apply a current step to the system, it will fire spikes with a sharp after-potential before converging to the fixed point where the system will present a broad after potential, therefore the system will present a typical transient phase corresponding to the initial bursting mode.

We conclude that if the neuron satisfies theorem 3.2, it will be in an adapting

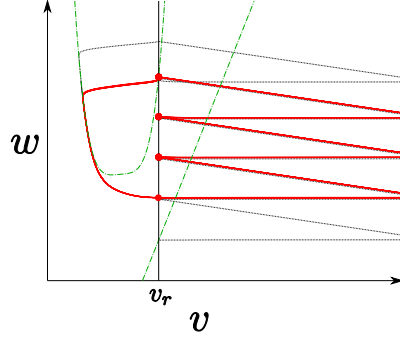


FIGURE 3.4. *Bursting generalized limit cycle. Trajectories are cut to a given threshold high enough to approximate the behavior of the system with explosion. The red curve corresponds to the bursting limit cycle, and the red circles the reset locations on this cycle. The black trajectory is the transient phase, and the green dotted curves correspond to the nullclines of the system.*

mode, and if not, it will be in an initial bursting mode. This criterion predicts the results numerically obtained by Naud and collaborators (23), as discussed in more details in section 5.2.

3.3. Tonic Bursting. As observed numerically in (25) and as we can see in figure 3.4, the bursting activity is linked with the existence of a generalized limit cycle of the hybrid system, the *bursting limit cycle*, virtually containing a few points having an infinite membrane potential. The regular bursting behavior, whatever the transient behavior, is related to the presence of such a cycle, and this cycle corresponds exactly to periodic orbits for the adaptation map Φ .

We can provide a condition for having cycles of any period. Indeed, one of the simplest application of Sarkovskii's theorem (see e.g. (5)) is that if there exists a periodic point of period 3, then there exist periodic points of any period, hence bursts with any number of spikes per burst. Theorem 3.4 provides a simple criterion on Φ to have a period 3 cycle.

THEOREM 3.4 (Cycles of any period). *Let $w_1 \stackrel{\text{def}}{=} \min\{\Phi^{-1}(w^*)\}$. Assume that:*

$$\begin{cases} \Phi(w^*) > w^* \\ \Phi^2(w^*) < w_1 \\ \Phi^3(w^*) > w^* \end{cases} \quad (3.6)$$

Then there exists a non-trivial period 3 cycle, hence the reset process has cycles of any period.

Proof. The only thing to prove is that there exists a point $x \in \mathbb{R}$ such that

$$\begin{cases} \Phi^3(x) = x \\ \Phi(x) \neq x \end{cases}$$

We know that there exists a unique fixed point of Φ , which we denote w_{fp} and which lies in the interval $[w^*, \Phi(w^*)]$. Here we prove that there exists another solution of $\Phi^3(x) = x$. Indeed, let us describe the function Φ^3 :

- It is increasing on $(-\infty, w_2)$ where $w_2 = \min\{\Phi^{-2}(w^*)\}$, and $\Phi^3(w) > w$ on this interval by concavity

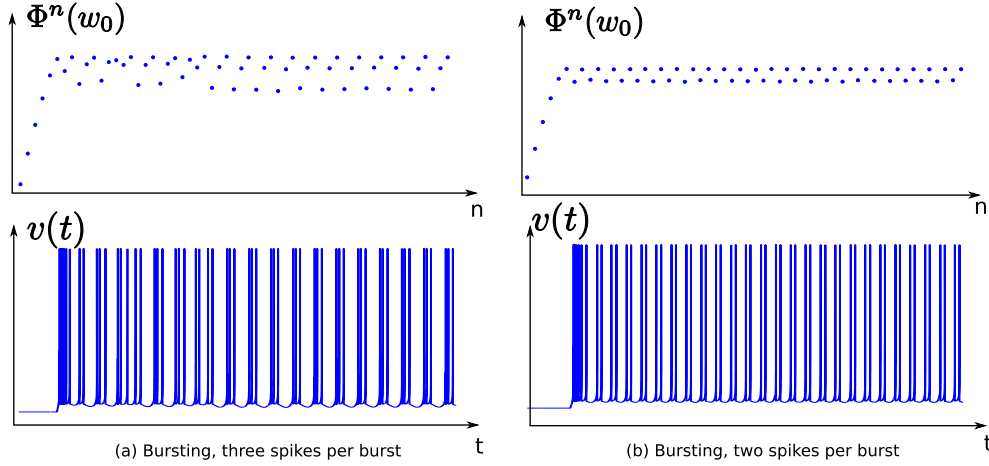


FIGURE 3.5. *Bursting in the quartic model: bursts with different number of spike per bursts and related periodic orbit of Φ .*

- decreasing on (w_2, w_1) and $\Phi^3(w_1) = \Phi^2(w^*) < w_1$ hence the curve crosses once the curve $y = x$, at a point strictly lower than w^* .

Hence we proved that there exists a period 3 cycle. Sarkovskii's theorem (see e.g. (5)) ensures us that there are cycles of any period for the map Φ . \square

REMARK. *This theorem gives us a simple condition on Φ to get period 3 cycles. This implies that the system has periodic points of any period, but also that it has an uncountable number of non asymptotically periodic points, which is referred as chaos in the paper of Li and Yorke (20). Nevertheless this property can be rather defined as topological chaos, and does not correspond to the usual definition of chaos in mathematics and in neuroscience where it is understood as sensitive dependency on the initial condition.*

Simple sufficient conditions such as the ones given in theorem 3.4 in the case of periodic points of period three can be provided to for cycles of any given period. The difficulty is to prove that these conditions are satisfied, since we have no closed form expression for the map Φ , and in this case numerical simulation is helpful. As we will see in section 3.4, the system will undergo a period-adding bifurcation structure with respect to the reset value of the membrane potential, and therefore bursts of many periods will be observed.

3.4. Dependency on the parameters. We have seen that in the case where the subthreshold dynamics has no fixed point, the spike patterns produced can correspond to tonic spiking or tonic bursting depending on the parameters of the system. The question we address in this section is to characterize the dependency of the spike patterns with respect to the parameters of the model, and the bifurcations from one behavior to the other.

3.4.1. Bifurcations with respect to the spike-triggered adaptation parameter. The parameter having the simplest effect on the dynamics is the spike-triggered adaptation parameter d : it simply shifts vertically (i.e. along the y -axis) the adaptation map, and does not modify its shape. This simple behavior allows us to understand qualitatively the changes in the behavior of the adaptation sequence.

First of all, note that the unique fixed point of the map Φ is an increasing function of the spike-triggered adaptation d . We denote it $w_{fp}(d)$.

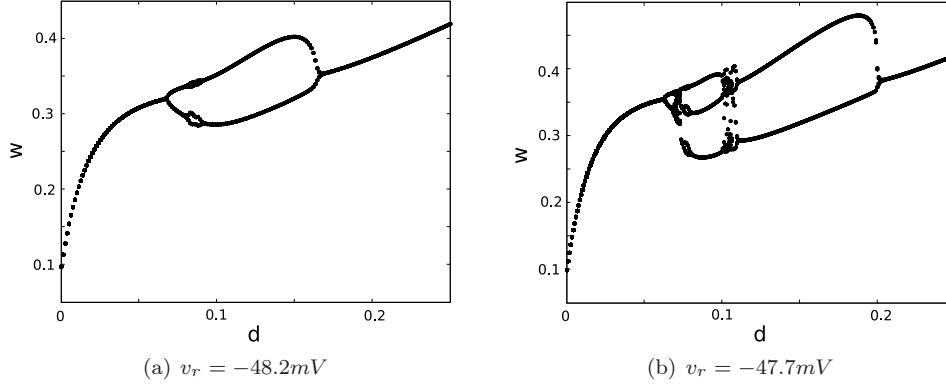


FIGURE 3.6. Orbits under Φ for different initial conditions, varying the spike-triggered adaptation parameter d , in the case of the dimensioned Adaptive Exponential model. We can observe that for d small enough the system converges towards the fixed point of Φ . When increasing d , as described in the text, the fixed point loses stability via a period doubling bifurcation and a cycle of period 2 appears. In the case (a) the system presents another period doubling bifurcation for $d \approx 0.8$, and then returns to equilibrium via an inverted period doubling bifurcation. In the second simulation for a larger value of v_r , the system involves chaotic spiking patterns.

If the adaptation map is globally contracting (i.e. $\max_{v \in \mathbb{R}} |\Phi'(v)| < 1$), we will not observe bifurcations in the parameter d , and the sequence will always converge to the unique fixed point.

If the map is not globally contracting, bifurcations can appear with respect to the parameter d . Denote by \mathcal{I}_1 the set of $w \in \mathbb{R}$ such that $|\Phi'(w)| > 1$. This set is a bounded closed set included in $[w^*, \infty)$, because of the convexity property of Φ and the presence of the plateau. Indeed, if $w_{fp} < w^*$, then since Φ is increasing we would have $0 < \Phi'(w_{fp}) < 1$. Furthermore, because of the plateau region, we have $\Phi'(w_{fp}(d)) \rightarrow 0$ when $d \rightarrow \infty$. As stated, since the shape of Φ does not depend on d , neither does \mathcal{I}_1 .

If $w_{fp}(0) > \max\{\mathcal{I}_1\}$, then the fixed point of the system is always stable for all $d > 0$ and there is no bifurcation in d .

If $w_{fp}(0) \in \mathcal{I}_1$, we denote by $d_1 = \inf\{d > 0; w_{fp}(d) \notin \mathcal{I}_1\}$. The fixed point will be unstable and the neuron will be bursting or chaotically spiking while $d < d_1$, and for $d > d_1$, the fixed point becomes stable and the neuron will fire regularly. At the point where $d = d_1$, the fixed point has a multiplier equal to -1 because of the negativity and continuity of the derivative, and the map undergoes a non-generic doubling bifurcation. The transversality condition (see e.g. (19, section 4.5)) is never satisfied since we have $\frac{\partial \Phi}{\partial d} \equiv 1$ (see equation (3.3)) and hence $\frac{\partial^2 \Phi}{\partial w \partial d} \equiv 0$.

If $w_{fp}(0) < \min\{\mathcal{I}_1\}$, we similarly define $d_1 = \inf\{d > 0, w_{fp}(d) \in \mathcal{I}_1\}$ and $d_2 = \sup\{d \geq d_1, w_{fp}(d) \in \mathcal{I}_1\}$. The system will undergo a degenerate period doubling bifurcation at the point $w_{fp}(d_1)$ for $d = d_1$ and a period doubling bifurcation at the point $w_{fp}(d_2)$ for $d = d_2$. For $d \in (d_1, d_2)$, the system does not have a stable fixed point. It can emit bursts, or even have a chaotic behavior in this zone (see figure 3.6).

3.4.2. Stabilization by the input current. The input current is a very interesting parameter, since it can be related to a biophysical value that can be controlled in *in vitro* experiments. Moreover, the set of input currents such that the system has no fixed point has a very simple shape, corresponding to the semi-infinite interval $(-m(b), \infty)$.

Interestingly, we prove that increasing the input current has a stabilizing effect on the behavior of the neuron: we prove in theorem 3.5 that for I large enough the adaptation sequence always converges to a fixed point.

THEOREM 3.5. *Let the parameters a, b, v_r, d be fixed. There exists I_s such that for all $I > I_s$ all orbits under Φ converges.*

Proof. The proof of this theorem is based on the changes induced by increasing the current around the point (v_r, w^*) . We prove that increasing I enough will make the system satisfy the hypothesis of theorem 3.2.

The point w^* depends on I , and therefore we denote it $w^*(I)$ in this proof for the sake of clarity. We change variables and consider $\hat{w} = w - I$. The change of variables maps w^* to $\hat{w}^* = F(v_r)$. The equations satisfied by (v, \hat{w}) are readily deduced from the original system, the new adaptation map can be written as:

$$\hat{\Phi}(\hat{w}) = \Phi(\hat{w} + I) - I,$$

and the condition of theorem 3.2 simply reads $\hat{\Phi}(\hat{w}^*) \leq \hat{w}^*$.

The equation of the trajectory in the phase plane (v, \hat{w}) for any initial condition in the spiking zone can be parametrized as a function of v : $\hat{w}(t) = \hat{W}(v(t), v_0, w_0, I)$, where \hat{W} satisfies the equation:

$$\begin{cases} \frac{\partial \hat{W}}{\partial v} = \frac{a(bv - \hat{W})}{F(v) - \hat{W}} - \frac{aI}{F(v) - \hat{W}} \stackrel{\text{def}}{=} \hat{g}(v, \hat{W}, I) \\ \hat{W}(v_0, v_0, w_0, I) = w_0 \end{cases}$$

Let $I_0 > -m(b)$ a fixed current, $\delta > 0$ a given real and $\Delta = d + 1$ where d is the spike-triggered adaptation parameter. Because of the shape of the vector field, the trajectories with initial condition (v_r, w^*) can be parameterized as a function of v with a singularity at $v = v_r$. We consider the trajectories on the interval $[v_r, v_r + \delta]$, and we prove that the infimum of the variable \hat{W} with initial condition (v_r, \hat{w}^*) , for $I \geq I_0$ and $v \in [v_r, v_r + \delta]$ is smaller than $F(v_r) - \Delta$.

To this end, let us characterize the orbits starting from this point (v_r, \hat{w}^*) as a function of the input current I . First of all, it is clear using Gronwall's theorem that $I \mapsto \hat{W}(v, v_r, \hat{w}^*, I)$ is decreasing. Therefore we have $\hat{W}(v_r + \frac{\delta}{2}, v_r, \hat{w}^*, I) \leq \hat{W}(v_r + \frac{\delta}{2}, v_r, \hat{w}^*, I_0) \stackrel{\text{def}}{=} \hat{w}_0$ and hence $\hat{W}(v_r + \delta, v_r, \hat{w}^*, I) \leq \hat{W}(v_r + \delta, v_r + \frac{\delta}{2}, \hat{w}_0, I)$.

Assume now that the infimum of \hat{W} for all $v \in [v_r + \frac{\delta}{2}, v_r + \delta]$ is greater than $F(v_r) - \Delta$. We have:

$$\hat{g}(v, \hat{W}, I) - \hat{g}(v, \hat{W}, I_0) = -\frac{a(I - I_0)}{F(v) - \hat{W}}$$

and hence:

$$\begin{aligned} \hat{W} &\geq F(v_r) - \Delta \\ F(v) &\leq \max_{v \in [v_r, v_r + \delta]} F(v) \\ F(v) - \hat{W} &\leq \max_{v \in [v_r, v_r + \delta]} F(v) - F(v_r) + \Delta \\ \frac{1}{F(v) - \hat{W}} &\geq \frac{1}{\max_{v \in [v_r, v_r + \delta]} F(v) - F(v_r) + \Delta} \\ -\frac{a(I - I_0)}{F(v) - \hat{W}} &\leq -\frac{a(I - I_0)}{\max_{v \in [v_r, v_r + \delta]} F(v) - F(v_r) + \Delta} \end{aligned}$$

which is constant and strictly negative. Therefore, using Gronwall's theorem, we have

$$\hat{W}(v_r + \delta, v_r, \hat{w}^*, I) - \hat{W}(v_r + \delta, v_r, \hat{w}^*, I_0) \leq -\frac{a(I - I_0)\delta}{\max_{v \in [v_r, v_r + \delta]} F(v) - F(v_r) - \Delta}$$

Therefore there exists I_1 such that for all $I > I_1$, we have $\min_{v \in [v_r, v_r + \delta]} \hat{W}(v) < F(v_r) - \Delta$. This contradicts the assumption that the infimum of \hat{W} for all $v \in [v_r + \frac{\delta}{2}, v_r + \delta]$ is greater than $F(v_r) - \Delta$. Hence there exists I_1 such that for all $I > I_1$, we have $\min_{v \in [v_r, v_r + \delta]} \hat{W}(v) < F(v_r) - \Delta$, which means in particular $\min_v W(v) < F(v_r) + I - \Delta$. This minimal value is reached when the trajectory crosses the w -nullcline, and denote by v_1 the value of the variable v at this crossing time. We have, for all $I > I_1$:

$$\begin{aligned} \Phi(w^*(I)) &= \lim_{v \rightarrow \infty} W(v) + d \\ &= W(v_1) + \int_{v_1}^{\infty} \frac{a(bv - W)}{F(v) - W + I} dv + d \end{aligned}$$

Moreover, we have $W(v) \geq bv_r$ for all v and $W(v) \leq bv$ for $v \geq v_1$. Therefore, we have:

$$\int_{v_1}^{\infty} \frac{a(bv - W)}{F(v) - W + I} dv \leq \int_{v_1}^{\infty} \frac{ab(v - v_r)}{F(v) - bv + I} dv.$$

The integrand is positive between v_r and v_1 , hence we have in particular:

$$\begin{aligned} \Phi(w^*(I)) &\leq F(v_r) + I - \Delta + d + \int_{v_r}^{\infty} \frac{ab(v - v_r)}{F(v) - bv + I} dv \\ &= F(v_r) + I - 1 + \int_{v_r}^{\infty} \frac{ab(v - v_r)}{F(v) - bv + I} dv \end{aligned}$$

The integrand tends to zero when $I \rightarrow \infty$ and is bounded by an integrable function (for instance the same function with $I = I_0$), hence by Lebesgue's theorem tends to 0 when $I \rightarrow \infty$. Therefore, there exists $I_s > I_0$ such that for all $I > I_s$, the integral is strictly smaller than 1, and therefore:

$$\Phi(w^*(I)) \leq F(v_r) + I = w^*(I).$$

Hence theorem 3.2 applies, which ends the proof. \square

Therefore, we can see that increasing the input current has a stabilizing effect on the dynamics. We present in figure 3.7 some numerical results illustrating this stabilization effect in the case of the exponential integrate-and-fire model. We observe for two different values of v_r that the system undergoes bifurcations with respect to the input current, sometimes involving chaotic spiking, but above a given value of the input current, the system spikes regularly, and the adaptation sequence converges towards its fixed point. Moreover, we have seen in the proof that when $I \geq I_s$, theorem 3.2 applies. Hence for I large enough, the system will present a spike frequency adaptation transient phase. Decreasing it will make the system switch to the case where there are two fixed points treated in section 4.

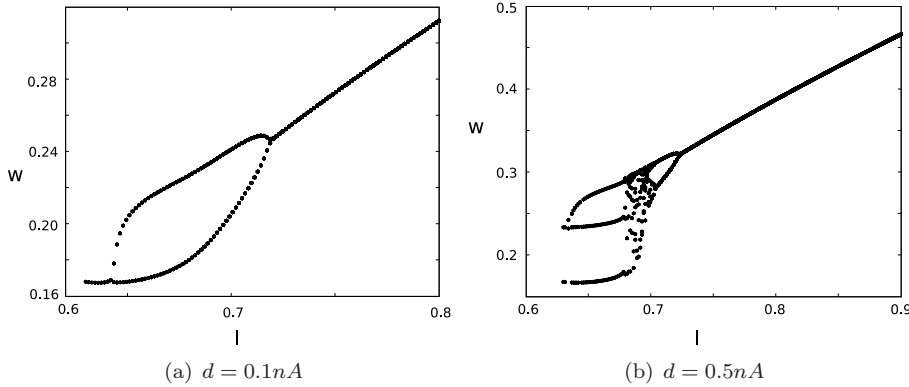


FIGURE 3.7. Orbits under Φ when varying the input current I in the case of the dimensioned Adaptive Exponential model. (a): Small v_r , the dynamics only presents a loss of stability via period doubling and then returns to equilibrium. (b): greater value of v_r : a period two cycle appears at the saddle-node current, immediately followed by a period 3 cycle, then via period-adding bifurcation the system returns to a period two cycle, and then by period doubling bifurcation to regular spiking. The transition from period three to period two shows a chaotic behavior.

3.4.3. Cascade of period adding bifurcations and chaos with respect to v_r . Another parameter preserving the number of fixed point is the reset value of membrane potential v_r . The dependency of the adaptation map with respect to this parameter is very intricate. The effect of increasing the reset value sharpens the adaptation map, and therefore can destabilize the possible stable fixed point or stable cycles. This qualitative observation is confirmed by numerical simulations. In the case of the exponential model, for v_r small enough, the adaptation map is smooth, because the slope of the exponential function for small v values tends to zero. But in the case of the quartic model, decreasing v_r also sharpens F because of the fast divergence of the quartic function.

We provide in figure 3.8 a graph of the stationary adaptation sequence (i.e. removing the transient phase) as a function of the reset voltage v_r corresponding to the quartic model. A similar diagram was given in the case of the adaptive exponential model in (27). We observe that the system present sharp transitions from rest (regular spiking) to cycles of period two (bursts with two spikes per burst) via a period doubling bifurcation, and from cycles of period n to cycles of period $n + 1$ for $n \geq 2$ via period adding bifurcations involving chaotic spiking regions.

3.5. Multistability. In section 3.2, we gave a sufficient condition on the map Φ for the convergence of the sequence (3.1) to the fixed point of Φ whatever the initial condition, which implies that the fixed point of Φ is stable and that its attraction basin is equal to \mathbb{R} . Nevertheless, in the case where the map Φ is not globally contracting, multistable behaviors could appear, corresponding to the coexistence of stable spiking orbits.

The study of periodic orbits is quite intricate in general systems, and this study in our case is even more complex since we do not have a closed form for the map Φ . We nevertheless observe numerically that cases of this type do not seem to occur: the stationary behavior of the adaptation sequence is the same whatever the initial condition.

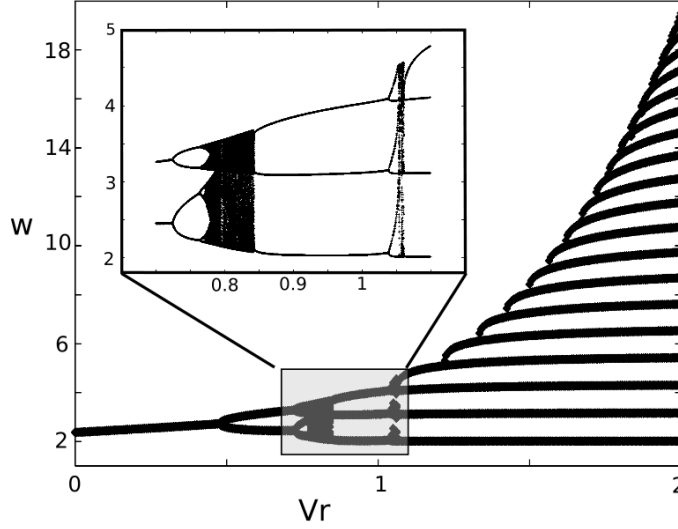


FIGURE 3.8. The period adding bifurcation cascade in the adaptation sequence for the quartic model, $a = 0.03$, $b = 0.7$, $d = 1.15$, and $v_r \in [0, 2]$, and a zoom on the transitions from period 2 to period 3 and period 3 to period 4. The same phenomenon appears in the adaptive exponential model, see (27).

4. Existence of fixed points. In the case where $I < -m(b)$, the system has two fixed points, one of which is always a saddle fixed point. We already studied in section 2 the stable manifold of this saddle fixed point (SMSFP) and explained in the cases where there exist SAs (fixed points or periodic orbit) how this manifold shaped the related attraction basin.

This stable manifold is essential for characterizing the definition domain and the dynamics of Φ . The map Φ will only be defined for values of w such that (v_r, w) is neither in the attraction basin of the possible SA nor on the SMSFP. We will study different cases in function of the topology of the intersection of the reset line with these sets, and mainly distinguish the cases where there is no intersection, finitely or countably many intersections or a continuous uncountable set of intersections.

4.1. Unconditional tonic behaviors. We are first interested in the cases where the reset line $\{v = v_r\}$ neither crosses the SMSFP nor the attraction basin of the possible SA. We know that the SMSFP is the graph of an unbounded increasing function of v for $v \geq v_+$ where v_+ is the greatest fixed point of the system. The cases where the SMSFP do not cross the reset line necessarily correspond to the cases where the stable manifold is included in a half plane $\{v \geq v_{\min}\}$. This corresponds to the cases where:

- the subthreshold system has two unstable fixed points and no stable limit cycle (Figs. 2.6(a) and 2.6(b)).
- an unstable limit cycle circles the stable fixed point (Fig. 2.5(a))
- the stable manifold crosses both nullclines (Fig. 2.5(b)).

In these cases, for all $v_r \leq v_{\min}$, the reset line does not intersect the SMSFP nor any possible attraction basin. Therefore, the adaptation map Φ is defined on \mathbb{R} and the proof of theorem 3.1 readily extends to this case. Hence in these cases Φ is a regular map increasing and concave on $(-\infty, w^*]$ and decreasing on $[w^*, \infty)$, having a unique

fixed point, a horizontal asymptote at infinity and such that $\Phi(w) \geq w + d$ for all $w \leq w^{**}$. Since the map Φ is defined on \mathbb{R} (and therefore $\Phi(\mathcal{D}) \subset \mathcal{D}$), if the neuron fires a spike, then it will fire infinitely many spikes. In that case, the map satisfies the same properties as when the subthreshold system has no fixed point, and theorems 3.2, 3.3 and 3.4 apply.

4.2. Phasic behaviors. In this section, we consider the cases where the reset line intersects the attraction basin \mathcal{B} of SA and denote by \mathcal{C} the SMSFP. The set of adaptation values on the reset line that do not lead the system to fire is given by:

$$\mathcal{A} = \{w \in \mathbb{R} ; (v_r, w) \in \mathcal{B} \text{ or } (v_r, w) \in \mathcal{C}\}.$$

The definition domain of the adaptation map in this case is

$$\mathcal{D} = \mathbb{R} \setminus \mathcal{A},$$

the set of initial conditions corresponding to a phasic spiking (i.e. emission of a finite number of spikes) is given by

$$P = \bigcup_{n=0}^{\infty} \Phi^{-n}(\mathcal{A})$$

and the complement of this set corresponds to the tonic spiking cases.

To study further the behavior of the system in this case, we discuss different cases depending on the shape of the stable manifold and the position of v_r with respect to the fixed point v_+ . Interestingly, the shape of the stable manifold only depends on the parameters of the subthreshold system.

4.3. The stable manifold Γ^- does not cross the v -nullcline. We first consider the case where the manifold Γ^- does not cross the v -nullcline. We distinguish two cases depending on whether $v_r \leq v_+$ or not.

PROPOSITION 4.1. *If the manifold Γ^- does not cross the v -nullcline and $v_r > v_+$, the manifold Γ^+ separating the spiking and non-spiking regions is the graph of an increasing function of v , and is above the two nullclines. The definition domain \mathcal{D} of the adaptation map Φ is an open interval $(-\infty, w_{\max}(v_r))$ with $w_{\max}(v_r) > w^*$ ($> w^{**}$). We denote $\Phi(w_{\max}(v_r)^-) \stackrel{\text{def}}{=} \lim_{w \rightarrow w_{\max}(v_r)} \Phi(w)$ the left limit of Φ at the point $w_{\max}(v_r)$. We have:*

- *If $\Phi(w_{\max}(v_r)^-) > w_{\max}(v_r)$ the system fires finitely many spikes whatever the initial condition in \mathcal{D} ,*
- *If $\Phi(w_{\max}(v_r)^-) < w_{\max}(v_r)$ and $\Phi(w^*) < w_{\max}(v_r)$ the system fires infinitely many spikes whatever the initial condition in \mathcal{D} ,*
- *Else, the system will either fire finitely or infinitely many spikes depending on the initial condition.*

Proof. First of all, we note that Φ satisfies the same properties on \mathcal{D} as the one given in theorem 3.1. The shape of the domain \mathcal{D} is readily deduced from the shape of the separatrix.

- In the case where $\Phi(w_{\max}(v_r)^-) > w_{\max}(v_r)$ (see figure 4.2(d)) there exists a real $\varepsilon > 0$ such that $\Phi(w) - w \geq \varepsilon$ for all $w \in \mathcal{D}$. Indeed, because of the monotony of Φ on $(w^*, w_{\max}(v_r))$ we have for all w in this interval $\Phi(w) \geq \Phi(w_{\max}(v_r)^-) > w_{\max}(v_r) \geq w$ and because of the convexity property of Φ and the fact that $\Phi(w) \geq w + d$ for all $w \leq w^{**}$, the distance between Φ and

the identity map is lowerbounded. Hence $\Phi(w) \geq w + \varepsilon$, and there exists $N > 0$ such that $\Phi^N(w) \geq w_{\max}(v_r)$, thus the system has a phasic spiking behavior (see figure 4.2(g)).

- In the case where $\Phi(w_{\max}(v_r)^-) < w_{\max}(v_r)$ and $\Phi(w^*) < w_{\max}(v_r)$ (see figure 4.2(c)), then we have $\Phi(\mathcal{D}) \subset \mathcal{D}$, since the maximum of the map Φ is reached at w^* , and therefore the system will fire infinitely many spikes. Depending on the properties of the map Φ and of its fixed point, the system can either spike regularly (when the fixed point is stable), generate bursting or chaotic spike patterns. Figure 4.2(g) corresponds to this case when the fixed point is stable and generates a regular spiking behavior.
- In the case where $\Phi(w^*) \geq w_{\max}(v_r)$, we do not have $\Phi(\mathcal{D}) \subset \mathcal{D}$. In this case, \mathcal{D} can be split into two different sets that can have quite intricate shapes: a set of values of the adaptation variable where the neuron fires finite many spikes and a set where the neuron fires infinitely many spikes. To study these sets, we define

$$P_1 = \{w \in \mathcal{D} ; \Phi(w) \geq w_{\max}(v_r)\}$$

This set corresponds to the set of adaptation values w such that $\Phi(w) \notin \mathcal{D}$ and hence that will fire one spike and then return to a subthreshold stable orbit. We then define recursively the set $P_{n+1} = \Phi^{-1}(P_n)$ of initial conditions such that the neuron will fire exactly $n + 1$ spikes before being attracted by the stable subthreshold orbit. The set of phasic spiking initial conditions is therefore defined by

$$P = \bigcup_{n=1}^{\infty} P_n,$$

and the set of tonic spiking is $\mathcal{D} \setminus P$. In figure 4.1 we represented the construction of these two sets until T_3 , and we observe the complexity of the set we will obtain. If the fixed point is stable, both the tonic spiking and the phasic spiking sets will be a countable union of non-empty intervals, and the adaptation sequence will jump from one interval to the other until reaching the attraction basin of the fixed point of Φ , where they keep trapped. If the fixed point is unstable, the tonic spiking set will be countable, defined by the union of the consecutive reciprocal images of the unstable fixed point under Φ . Therefore the neuron will not present cycles. In this case, the behavior of Φ strongly depends on the initial condition.

□

PROPOSITION 4.2. *If $v_r \leq v_+$ and Γ^- does not cross the v -nullcline, the definition domain \mathcal{D} is an open interval $(-\infty, w_{\max}(v_r))$ with $w_{\max}(v_r) \leq w^*$. The neuron fires infinitely many spikes if and only if $\Phi(w_{\max}(v_r)^-) \leq w_{\max}(v_r)$. In this case the neuron is in a regular spiking mode with spike frequency adaptation.*

Proof. If $v_r \leq v_+$ and Γ^- does not cross the v -nullcline, it is clear that the definition domain \mathcal{D} of the adaptation map Φ is an open interval $(-\infty, w_{\max}(v_r))$ where $w_{\max}(v_r) \leq w^*$ is the value of the adaptation variable at the intersection point of the reset line with Γ^- . The maximal value of Φ on its definition domain is given by $\Phi(w_{\max}(v_r)^-)$.

- if $\Phi(w_{\max}(v_r)^-) \leq w_{\max}(v_r)$, then we have $\Phi(\mathcal{D}) \subset \mathcal{D}$ and hence the system is always in a regular spiking mode if it fires one spike. Moreover, the proof

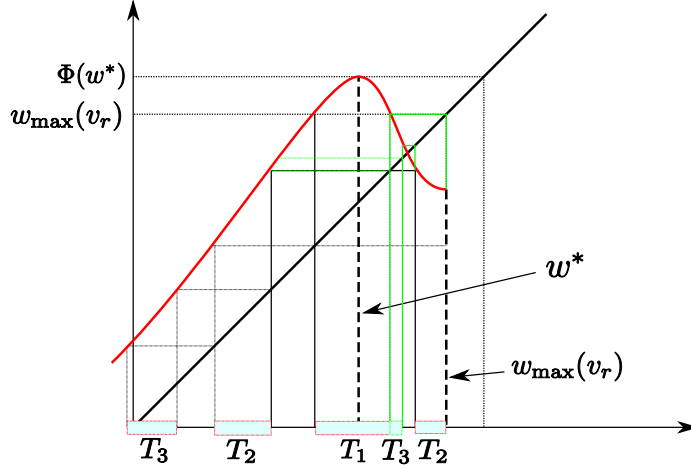


FIGURE 4.1. Construction of the phasic spiking set in the case of an unbounded separatrix when $\Phi(w^*) > w_{\max}$, for three iterations. The red curve is the map Φ and the black line the first bisector. The green construction line correspond to the contribution of the set T_2 for $w > w^*$ to T_3 .

of theorem 3.2 readily extends to the present case and therefore the system will be in a regular spiking mode with spike frequency adaptation.

- If $\Phi(w_{\max}(v_r)^-) > w_{\max}$, because of the convexity property (which can be proved in exactly the same way as in theorem 3.1), there exists $\varepsilon > 0$ such that $\Phi(w) - w \geq \varepsilon$ and therefore the system will return to rest after firing finitely many spikes.

□

In the case where Γ^- intersects no nullcline (e.g. in the case of figure 4.2(a)), we will have $w_{\max}(v_r) \leq w^*$ and hence $\Phi(w_{\max}(v_r)^-) \geq w_{\max}(v_r) + d$, hence the system will always be in a phasic spiking mode. In the tonic spiking cases of propositions 4.1 and 4.2 the system presents a bistable behavior: a stable subthreshold behavior and a stable spiking one coexist.

4.3.1. The stable manifold Γ^- crosses the v -nullcline. If the stable manifold crosses the v -nullcline as in figure 2.5(b), then there exists $v_{\min} \leq v_-$ such that the SMSFP is included in the half plane $\{v \geq v_{\min}\}$. For each $v \leq v_{\min}$, we have $\mathcal{D} = \mathbb{R}$ and the results of section 4.1 apply. For $v \geq v_{\min}$, the spiking behavior of the system satisfies the following:

PROPOSITION 4.3.

For $v \geq v_{\min}$, the reset line intersects the attraction basin on a bounded interval $(w_{\min}(v_r), w_{\max}(v_r))$ and the definition domain of the adaptation map is the union of two semi-infinite intervals:

$$\mathcal{D} = (-\infty, w_{\min}(v_r)) \cup (w_{\max}(v_r), \infty) \stackrel{\text{def}}{=} \mathcal{I}_1 \cup \mathcal{I}_2.$$

The spiking pattern satisfies the following classification (see figure 4.3):

- If $\sup_{w \in \mathcal{I}_1} \Phi(w) \in [w_{\min}(v_r), w_{\max}(v_r)]$, the system fires finitely many spikes
- If $\sup_{w \in \mathcal{I}_1} \Phi(w) < w_{\min}(v_r)$, the system fires infinitely many spikes. If $v_r \leq v_+$, the system presents regular spiking with spike frequency adaptation.
- If $\sup_{w \in \mathcal{I}_1} \Phi(w) > w_{\max}(v_r)$, the system fires finitely or infinitely many spikes depending on the initial condition.

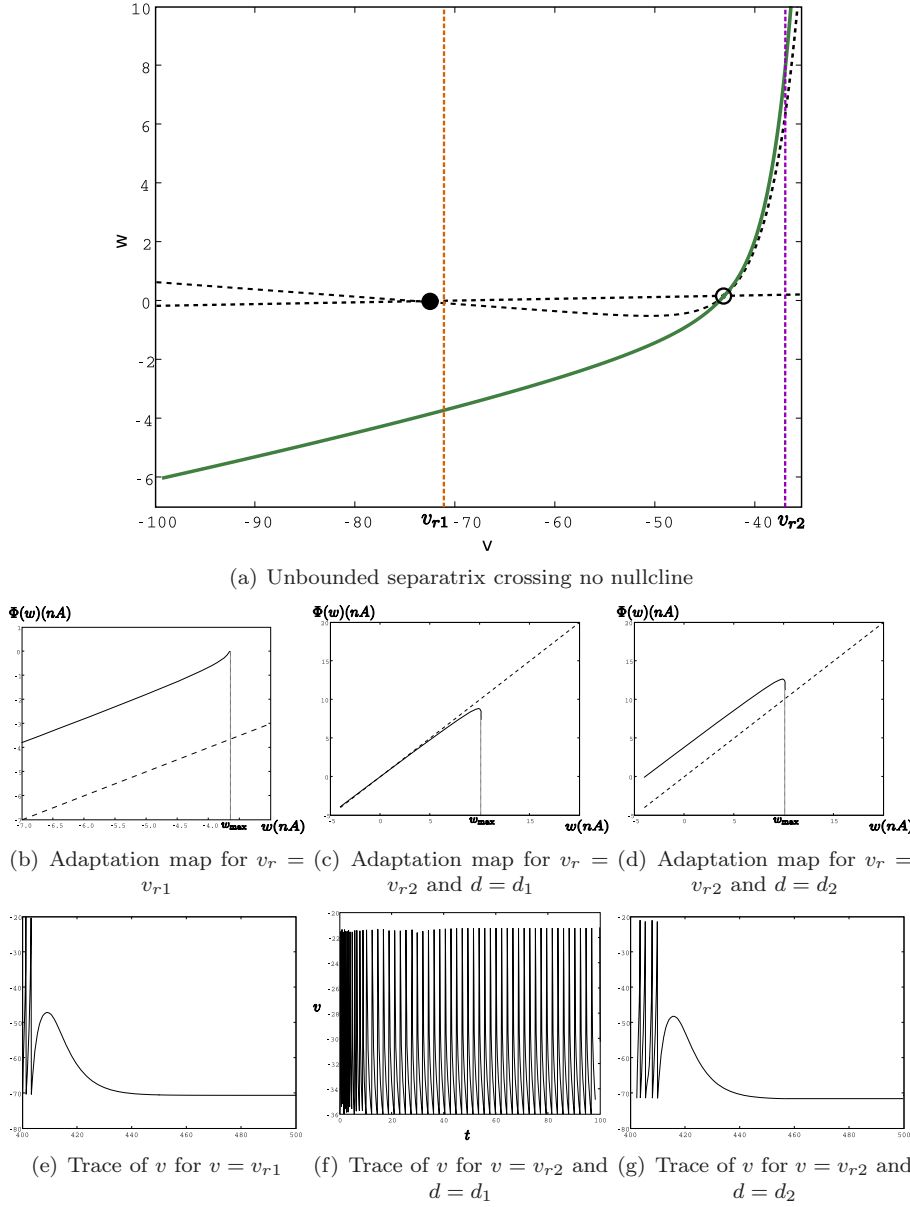


FIGURE 4.2. Case of an unbounded separatrix: unconditional phasic behavior for $v < v_-$. In the case $v > v_+$, the behavior can either be phasic or tonic depending on the parameters of the system. It can also depend on the initial condition. Case of the adaptive exponential model, original parameters, $a = .2g_L$ and $\tau_w = \tau_m/3$, $d_1 = 0.01nA$ and $d_2 = 3nA$. We chose $v_{r1} = -70.6mV$ (value of the original model) and $v_{r2} = -36mV$ which is unrealistically high for biological applications, and results in very fast spiking behaviors as in the case of figure (f).

Proof. The shape of the domain \mathcal{D} is a direct consequence of the assumption on Γ^- . First of all, we note that any orbit starting from (v_r, w) with $w \in \mathcal{I}_2$ will cross the reset line on \mathcal{I}_1 after a finite time, and therefore we have $\Phi(\mathcal{I}_2) \subset \Phi(\mathcal{I}_1)$.

- If $\sup_{w \in \mathcal{I}_1} \Phi(w) \in [w_{\min}(v_r), w_{\max}(v_r)]$ (see figure 4.3(a)), then there exists

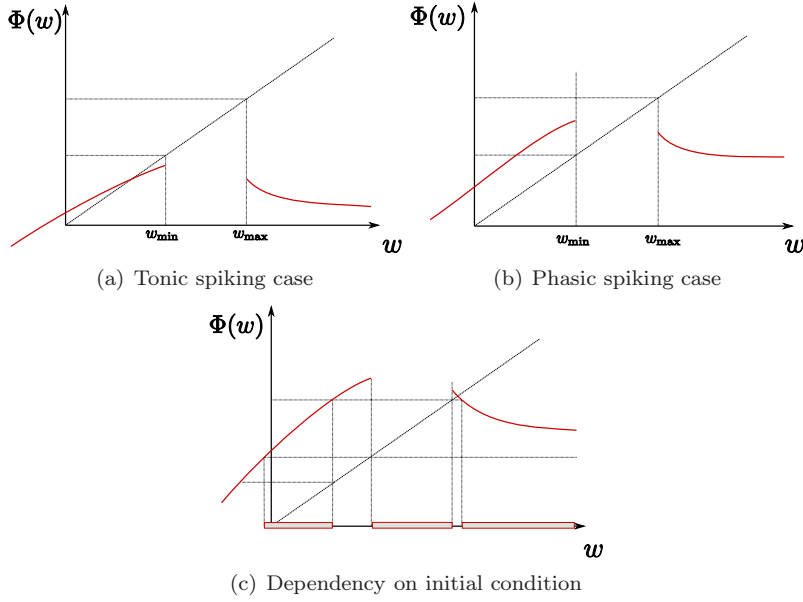


FIGURE 4.3. Case where the SMSFP crosses the v -nullcline, in the case of the quartic model, $a = 1$, $b = 2.5$, $I = -0.5$, $v_r = 0$ and different values of d . (a): Tonic spiking mode, the adaptation sequence converges towards the fixed point of Φ . (b): Phasic spiking mode: for any initial condition the adaptation sequence will enter the zone $[w_{\min}, w_{\max}]$ and the neuron stops firing. (c): the spiking behavior is tonic or phasic depending on the initial condition. The blue boxes represent the zones of initial conditions related to a phasic behavior with zero or one spikes emitted.

$\varepsilon > 0$ such that $\sup_{w \in \mathcal{I}_1} \Phi(w) - w \geq \varepsilon$ and therefore any orbit will exit \mathcal{D} and enter the subthreshold orbits set after firing few spikes. For any initial condition $w \in \mathcal{I}_2$ we have $\Phi(w) \subset \Phi(\mathcal{I}_1)$ and therefore either $\Phi(w)$ is in the attraction basin of the subthreshold equilibrium, or it is in \mathcal{I}_1 and the above analysis applies and the system is in a phasic spiking mode.

- If $\sup_{w \in \mathcal{I}_1} \Phi(w) < w_{\min}(v_r)$ (see figure 4.3(b)), then necessarily $\Phi(\mathcal{I}_1) \subset \mathcal{I}_1$ and the map Φ has a fixed point in \mathcal{I}_1 . Furthermore, we have $\Phi(\mathcal{D}) \subset \mathcal{I}_1$ and therefore the system will be in a tonic spiking behavior. If $v_r \leq v_+$, we have $w_{\min} < w^*$, the fixed point is attracting and for any initial condition the adaptation sequences converge to this fixed point (see proof of theorem 3.2). Moreover in that case the transient phase is characterized by spike frequency adaptation.

If $v_r > v_+$, the type of tonic spiking depends on the properties of the map, the system is in a regular spiking mode with initial bursting, a bursting mode or a chaotic spiking mode.

- If $\sup_{w \in \mathcal{I}_1} \Phi(w) > w_{\max}(v_r)$ (see figure 4.3(c)), then there exists an interval $J \subset \mathcal{D}$ such that all the trajectory with initial condition (v_r, w) with $w \in J$ will stop firing after one spike. We can build the phasic and the tonic subspaces of \mathcal{D} recursively as done in the previous case. The shape of this set can be quite complex, and the behavior of the adaptation sequence depends on the initial condition on this set.

□

4.3.2. Bounded attraction basin. In the case where the attraction basin of the SA is delineated by a periodic orbit, we denote by v_{\min} the minimal value of the membrane voltage on the cycle and by v_{\max} its maximal value. The behavior of the system for $v_r \in (v_{\min}, v_{\max})$ is very complex. Indeed, the reset line will cross the attraction basin on an interval of values for the adaptation (w_{\min}, w_{\max}) , but since the stable manifold spirals around the orbit and converges to it, there is a countable sequence of intersection points of the reset line with the stable manifold: $(m_i, i \in \mathbb{N})$ converging to w_{\min} and $(M_i, i \in \mathbb{N})$ converging to w_{\max} . At each of these points the map Φ is undefined and there is a jump of the values of the map Φ . Hence the definition domain of the map Φ has a complex shape, and Φ an intricate discontinuous dynamics on it.

For $v_r > v_{\max}$ the reset line will cross the stable manifold on a finite set of adaptation values, and at these points the map Φ is undefined and has a unique discontinuity, case we now generalize and study.

4.4. Case $\mathcal{D} = \mathbb{R} \setminus \mathcal{A}$ where \mathcal{A} is a finite or countable set. The case where the reset line crosses the SMSFP but not any attraction basin of SA is more intricate (see figure 4.4). It corresponds to the cases where:

- the subthreshold system has two unstable fixed points and no stable limit cycle, and $v_r \geq v_{\min}$ (cases of Figures 2.6(a) and 2.6(b)). When the stable manifold oscillates around the fixed point, there is a countably many intersection points.
- the subthreshold system has a stable fixed point and an unstable periodic orbit. In that case let us denote by $v_{p,\max}$ (respectively $v_{p,\min}$) the maximal (respectively minimal) value of the variable v or the periodic orbit. The line $\{v = v_r\}$ crosses the SMSFP but not the attraction basin when $v_{\min} \leq v_r < v_{p,\min}$ or $v_r \geq v_{p,\max}$.

In these two cases, the reset line $\{v = v_r\}$ has finitely many intersections with the stable manifold (except if $v_r = v_-$), and we denote by \mathcal{A} the set of intersection points. The map Φ is defined on $\mathbb{R} \setminus \mathcal{A}$. This set is a finite union of open intervals. On each interval, the map Φ satisfies the properties given in theorem 3.1 for the same reasons as the ones given in the related proof. At the intersection points of the reset line with the SMSFP, the shape of the orbits of the differential system (1.1) changes, and this implies that at these points the map Φ is discontinuous.

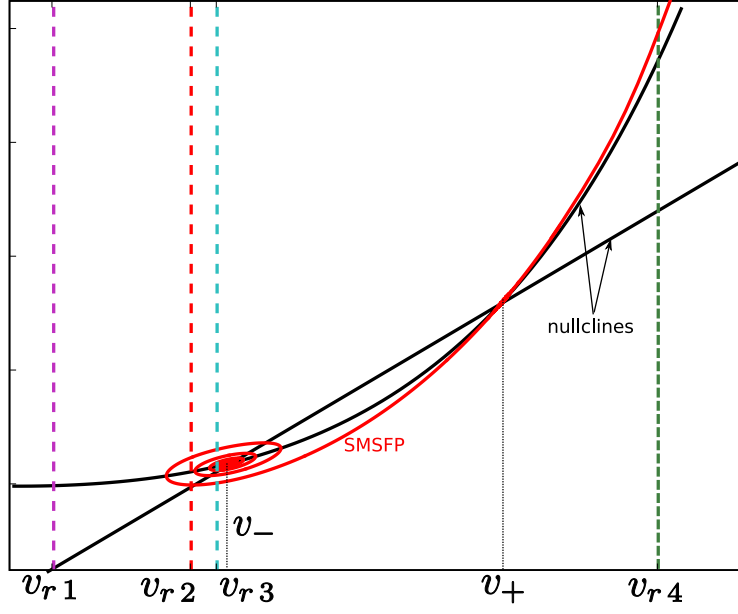
If $v_r > v_+$ then the map Φ will have a unique discontinuity point where the map is undefined (see figure 4.4(e)). For $v_{\min} < v_r < v_-$ it will have an odd number of such points (figures 4.4(c) and 4.4(d)) and for $v_r > v_-$, an even number. In the case where the Jacobian matrix has complex eigenvalues at the equilibrium v_- , the Poincaré map will have an infinite countable set of discontinuity points for $v_r = v_-$. The dynamics of Φ in this region of parameters will therefore be very complex. It can have multiple fixed points, no fixed point, and the map is discontinuous.

The set of adaptation values such that the system stops firing after a finite number of spikes emitted (phasic spiking regime) is given by:

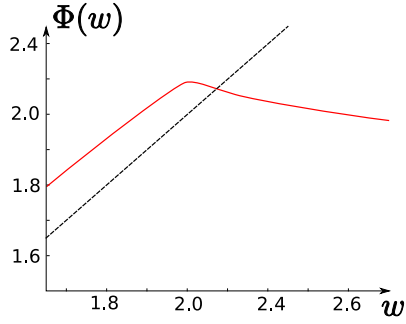
$$\bigcup_{n=0}^{\infty} \Phi^{-n}(\mathcal{A})$$

It is the set of initial conditions such that the orbits are exactly on the SMSFP after a finite number of iterations.

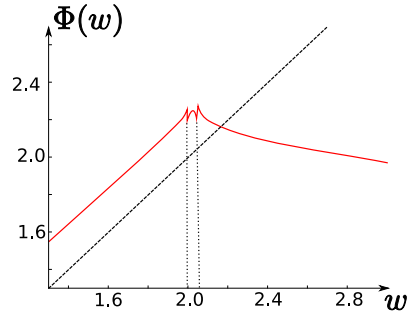
Therefore, the topology and the dynamics of Φ on these sets is quite complex. The related spiking sequence is also extremely complex in these cases:



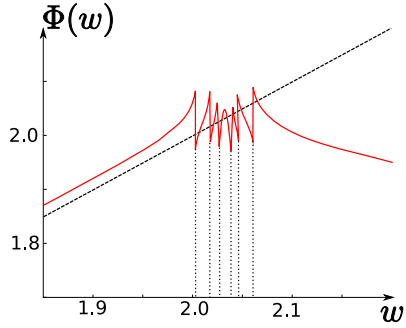
(a) Nullclines and different reset locations $v_{r1}, v_{r2}, v_{r3}, v_{r4}$ corresponding to different qualitative behaviors for the map Φ .



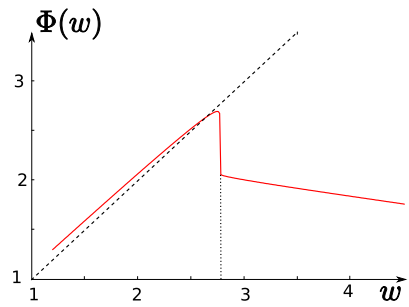
(b) $v_r = v_{r1}$: Φ is continuous



(c) $v_r = v_{r2}$: 2 discontinuity points



(d) $v_r = v_{r3}$: 6 discontinuity points, 7 fixed points



(e) $v_r = v_{r4}$: 1 discontinuity point

FIGURE 4.4. Case of two unstable fixed points for the classical adaptive exponential model. Phase plane and graph of the map Φ for different values of v_r , for the same set of parameters.

- If the map Φ has not fixed point, regular spiking is impossible, and the system will either present bursts or irregular spiking.
- If there is a unique fixed point, then regular spiking and bursts can coexist depending on the initial condition on the reset line.
- The case where there are many fixed points (see figure 4.4(d)) is even more complex. In this case the system could have different regular spiking frequencies, depending on the initial condition. In this case of multiple attractors, the system could switch between these attractors, be chaotic, present hysteresis and its sensitivity increases.

5. Discussion.

5.1. Physiological relevance. The first two-dimensional spiking neuron model with diverging spiking dynamics was introduced by Izhikevich (15), who showed that these models could qualitatively reproduce many different electrophysiological features of real neurons, such as spike-frequency adaptation, bursting, resonance, rebound spiking. . . A variation of that model, the adaptive exponential integrate-and-fire model (3), includes an exponential spike initiation current (11), which is a realistic approximation of the sodium current (whose activation function is a Boltzmann function). That model (and variants) is able to quantitatively predict the responses of real neurons to injected currents in terms of spike times, with a millisecond precision (1; 4; 18). The quartic model (25) is another variant which can exhibit sustained subthreshold oscillations. Thus, a mathematical analysis of those models has direct biological relevance. That analysis was first addressed in (25; 27), mainly in terms of subthreshold dynamics. Here we studied the patterns of spikes, which correspond to orbits under the adaptation map.

Dynamical properties of that map can be related to electrophysiological features of the neuron model. When the differential system has a stable fixed point, orbits are generally finite, i.e., a finite number of spikes are emitted, which is called *phasic spiking* (one spike) or *phasic bursting* (several spikes). In some situations, typically when the reset value is high, finite and infinite orbits can coexist, i.e., the system is bistable.

When the differential system has no stable fixed point, orbits are infinite, an infinite number of spikes are emitted, which is called *tonic spiking*. This is the most interesting aspect of the dynamics, where we must look at the properties of the adaptation map. When orbits converge to a fixed point of that map, spikes become regularly spaced, which corresponds electrophysiologically to the *regular spiking* behavior. Thus, theorem 3.2 provides conditions under which the neuron model has a regular spiking behavior. Periodic orbits translate to repeating spike patterns, which corresponds electrophysiologically to the *bursting* behavior, where the period is the number of spikes per burst. The existence of fixed points or periodic orbits depends in a complex way on the parameters. In particular, a period-adding bifurcation structure appears when increasing the reset parameter. It is particularly interesting to see that these two-dimensional models can exhibit chaos, whose electrophysiological signature is irregular spiking. Chaos has been observed in higher dimensional continuous neuron models such as the Hodgkin-Huxley model and variants (10; 13; 24). It has also been observed in real neurons in vitro, such as the Purkinje cell (9; 14; 21; 22), where period doubling was observed in experiments when increasing the temperature with a fixed input current.

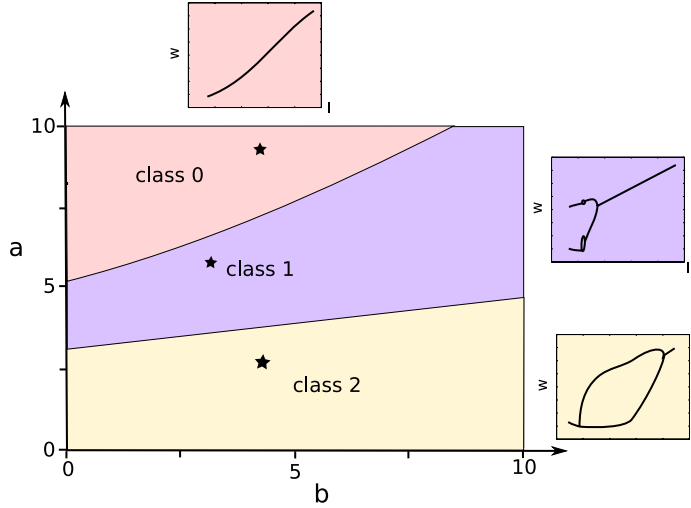


FIGURE 5.1. Electrophysiological classes for the quartic model with $d = 10$ and $v_r = 1$, as a function of the parameters a and b . Class 2 disappears when d is small enough. Both classes 1 and 2 disappear when v_r is close to the minimum of F (or small enough in the case of the exponential model). Sample members of these classes have been represented in the small figures around the classification figure: we represented the adaptation sequence after a given elapsed time, as a function of the input current. Parameters are marked with stars: class 0: $a = 8.5$, $b = 4.5$, class 1: $a = 6$, $b = 3.2$, and class 2: $a = 2.5$, $b = 4.5$.

5.2. Classifications. In (27), the authors defined electrophysiological classes for the subthreshold dynamics in the case of the adaptive exponential model². These classes are sets of parameters such that the neuron has the same qualitative behavior in response to different levels of input currents. We know that when I is smaller than $-m(b)$ the neuron will be in a phasic spiking behavior and when I is large enough, it will fire regularly. Classes are therefore distinguished depending on what is happening between these two stages, and three cases are possible:

0. The neuron always fires regularly (no transition).
1. The neuron first bursts then fires regularly (1 transition, see e.g. figure 3.7(b)).
2. The neuron fires regularly, then bursts, then fires regularly again (2 transitions, see e.g. figure 3.7(a)).

Classes 0 and 1 are observed in general whatever v_r and d for given values of a and b . Class 2 exists less often, and is generally observed for large values of the spike triggered adaptation d . We numerically compute the transitions between regular spiking and bursting. In Figure 5.1 we represented the number of transitions (i.e. the class of neuron) as a function of the parameters a and b for different pairs (v_r, d) .

Let us now be more specific and define zones of parameters corresponding to a unique given behavior. The criteria for regular spiking given in theorems 3.2 and 3.3 rely on some very simple properties of the map Φ . We apply here the results of these theorems in order to define sets of parameters corresponding to different classes of behaviors: regular spiking with spike frequency adaptation, regular spiking with initial bursting, burst of period two, and a class of burst of unspecified period and chaotic spiking. The case where theorem 3.2 applies corresponds to the case of regular

²their classification readily generalizes to the whole class of models we study here

spiking with spike frequency adaptation. In the case where theorem 3.3 applies, we check the stability of the fixed point of Φ by computing the related multiplier: if it is smaller than one in absolute value, the system is in a regular spiking mode with initial bursting, and if not, the neuron fires bursts of period two. Eventually, in the cases where none of the theorems applies, the system is necessarily in a bursting or chaotic mode.

We have seen that when I is high enough or when d is high enough, the neuron fires regularly. Figure 5.2(c) helps us specify the parameter sets related to regular spiking (with initial bursting or spike frequency adaptation) and bursting. We observe in figure 5.2(c) that the input current has a stabilizing effect on the whole dynamics: we simulated a case where the map Φ is not globally contracting for input currents close to $-m(b)$. When increasing the current, we observe that the map becomes globally contracting when the input current is high enough, which results in a regular spiking behavior. Therefore the electrophysiological class depends on d .

Another pair of interesting parameters is the pair of reset parameters (v_r, d) . The influence of these two parameters was numerically studied by Naud and collaborators in the case of the dimensioned adaptive exponential model (see (23)) for a current value twice the value of the saddle-node bifurcation current. They numerically simulated the spike trains and classified them as chaotic spiking, bursting, regular spiking with spike frequency adaptation and initial bursting. The mathematical criteria we have presented predict these zones, as shown on figure 5.2.

5.3. Perspectives. In this paper we studied the spike patterns produced by neurons in the class of models introduced in (25) in the case where the spike is emitted when the membrane potential blows up. We introduced a discrete map called the adaptation map, which is a generalization of the usual Poincaré applications in dynamical systems corresponding to the case where the Poincaré section is set at infinity. The rigorous mathematical study of this map allowed us to distinguish between the different spike patterns fired, and to derive simple criteria to characterize different spiking regimes of the neuron. These criteria can be easily applied in order to derive classes of parameters corresponding to different kinds of behaviors. We also proved that the system presented bifurcations as a function of the reset value of the membrane potential.

This study of a hybrid dynamical system opens the way to the study of different spiking models, such as bidimensional compartment models or bidimensional spiking models with or without explosion. In particular, this study readily applies to the case of Izhikevich' quadratic integrate-and-fire model which is a bidimensional nonlinear spiking neuron model where spikes are emitted when the membrane potential reaches a finite threshold. This framework may also be interesting in other fields of applied mathematics, and in particular in mathematical biology, ecology, economy and generally in any nonlinear system where discrete events occur depending on the state of the variables of the system.

Acknowledgments. The authors warmly acknowledge Olivier Faugeras and Wulfram Gerstner for interesting discussions. This work was partly supported by funding of the European Union under the grant no. 15879 (FACETS).

References.

- [1] LAURENT BADEL, SANDRINE LEFORT, ROMAIN BRETTE, CARL C. H. PETERSEN, WULFRAM GERSTNER, AND MAGNUS J. E. RICHARDSON, *Dynamic i-v curves are reliable predictors of naturalistic pyramidal-neuron voltage traces*,

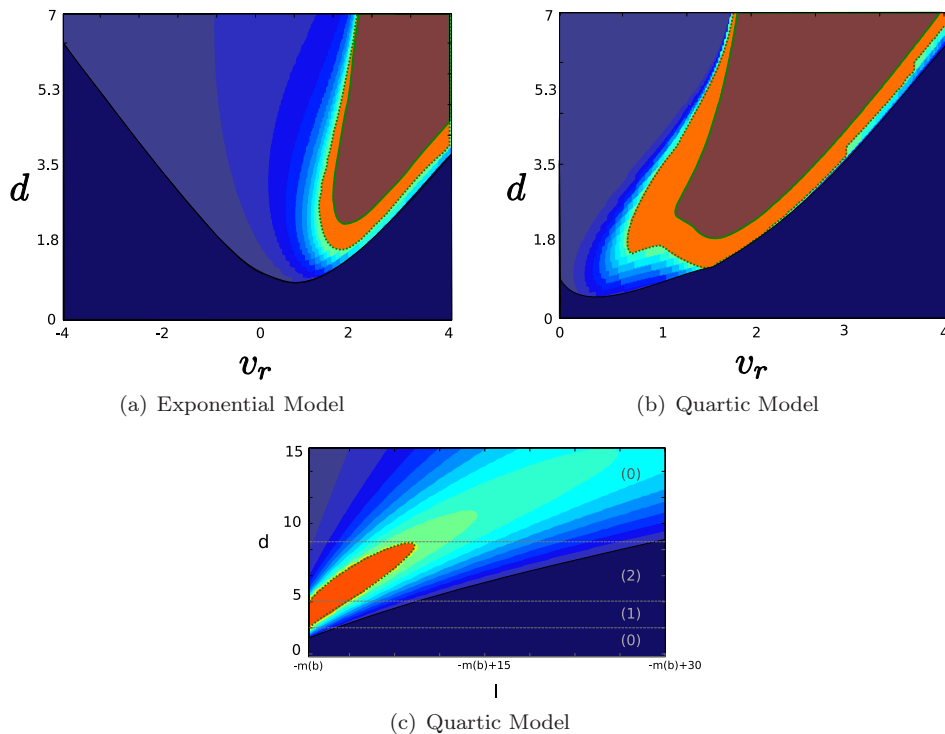


FIGURE 5.2. Zones of parameters corresponding to different spiking behaviors. (a): Reduced adaptive exponential model with $a = 1$, $b = 2$ and $I = 3$. (b): Quartic model, $a = 1$, $b = 2$, $I = -m(b) + 2$. (c): $a = 1$, $b = 1$, $v_r = 1.5$. Regular spiking is indicated in blue. The dark blue zone corresponds to spike frequency adaptation, and the other blue regions correspond to initial bursting. The color intensity is proportional to the multiplier of the fixed point: the smaller the multiplier the darker the region. The separatrix we obtain in figure (a) is very close to the one found numerically by Naud and collaborators in (23). Bursts and chaotic spiking are indicated in red/orange. The orange region corresponds to bursts with two spikes per burst (according to theorem 3.3). The green dotted line corresponds to the period doubling bifurcation. The brown zone corresponds to burst and chaos and the green solid line corresponds the initiation of the cascade of period doubling at the transition from period two to period three. In (c) the electrophysiological classes are represented as a function of d .

Journal of Neurophysiology, 99 (2008), pp. 656–66. PMID: 18057107 doi: 01107.2007.

- [2] ROMAIN BRETTE, *The cauchy problem for one-dimensional spiking neuron models*, Cognitive Neurodynamics, 2 (2007), pp. 21–27.
- [3] R. BRETTE AND W. GERSTNER, *Adaptive exponential integrate-and-fire model as an effective description of neuronal activity*, Journal of Neurophysiology, 94 (2005), pp. 3637–3642.
- [4] C. CLOPATH, R. JOLIVET, A. RAUCH, H.R. LÜSCHER, AND W. GERSTNER, *Predicting neuronal activity with simple models of the threshold type: Adaptive Exponential Integrate-and-Fire model with two compartments*, Neurocomputing, 70 (2007), pp. 1668–1673.
- [5] R.L. DEVANEY, *An Introduction to Chaotic Dynamical Systems*, Westview Press, 2003.
- [6] A. DHOOGHE, W. GOVAERTS, AND Y.A. KUZNETSOV, *Numerical Continuation*

- of *Fold Bifurcations of Limit Cycles in MATCONT*, Proceedings of the ICCS, (2003), pp. 701–710.
- [7] A. DHOOGHE, W. GOVAERTS, AND YU. A. KUZNETSOV, *Matcont: A matlab package for numerical bifurcation analysis of odes*, ACM Trans. Math. Softw., 29 (2003), pp. 141–164.
 - [8] JEAN DIEUDONNÉ, *Éléments d'analyse - Tome I : Fondements de l'analyse moderne*, Gauthier-Villars, 1963.
 - [9] Y. ETZION AND Y. GROSSMAN, *Potassium currents modulation of calcium spike firing in dendrites of cerebellar Purkinje cells*, Experimental Brain Research, 122 (1998), pp. 283–294.
 - [10] U. FEUDEL, A. NEIMAN, X. PEI, W. WOJTENEK, H. BRAUN, M. HUBER, AND F. MOSS, *Homoclinic bifurcation in a Hodgkin–Huxley model of thermally sensitive neurons*, Chaos: An Interdisciplinary Journal of Nonlinear Science, 10 (2000), p. 231.
 - [11] N. FOURCAUD-TROCME, D. HANSEL, C. VAN VREESWIJK, AND N. BRUNEL, *How Spike Generation Mechanisms Determine the Neuronal Response to Fluctuating Inputs*, Journal of Neuroscience, 23 (2003), p. 11628.
 - [12] T. H. GRONWALL, *Note on the derivative with respect to a parameter of the solutions of a system of differential equations*, Annals of Mathematics, 20 (1919), pp. 292–296.
 - [13] J. GUCKENHEIMER AND R.A. OLIVA, *Chaos in the hodgkin–huxley model*, SIAM Journal on Applied Dynamical Systems, 1 (2002), p. 105.
 - [14] J. HOUNSGAARD AND J. MIDTGAARD, *Synaptic control of excitability in turtle cerebellar Purkinje cells.*, The Journal of Physiology, 409 (1989), p. 157.
 - [15] E. IZHIKEVICH, *Simple model of spiking neurons*, IEEE Transactions on Neural Networks, 14 (2003), pp. 1569–1572.
 - [16] E.M. IZHIKEVICH, *Which model to use for cortical spiking neurons?*, IEEE Trans Neural Netw, 15 (2004), pp. 1063–1070.
 - [17] EUGENE M IZHIKEVICH AND GERALD M EDELMAN, *Large-scale model of mammalian thalamocortical systems.*, Proc Natl Acad Sci U S A, 105 (2008), pp. 3593–3598.
 - [18] R. JOLIVET, R. KOBAYASHI, A. RAUCH, R. NAUD, S. SHINOMOTO, AND W. GERSTNER, *A benchmark test for a quantitative assessment of simple neuron models*, Journal of Neuroscience Methods, 169 (2008), pp. 417–424.
 - [19] YURI A. KUZNETSOV, *Elements of Applied Bifurcation Theory*, Applied Mathematical Sciences, Springer, 2nd ed., 1998.
 - [20] T.Y. LI AND J. YORKE, *Period three implies chaos*, American Mathematical Monthly, 82 (1975), pp. 985–992.
 - [21] R. LLINAS AND M. SUGIMORI, *Electrophysiological properties of in vitro Purkinje cell somata in mammalian cerebellar slices*, The Journal of Physiology, 305 (1980), pp. 171–195.
 - [22] Y. MANDELBLAT, Y. ETZION, Y. GROSSMAN, AND D. GOLOMB, *Period Doubling of Calcium Spike Firing in a Model of a Purkinje Cell Dendrite*, Journal of Computational Neuroscience, 11 (2001), pp. 43–62.
 - [23] R NAUD, N MACILLE, C CLOPATH, AND W GERSTNER, *Firing patterns in the adaptive exponential integrate-and-fire model*, Biological Cybernetics, 99 (2008), pp. 335–347.
 - [24] J. RINZEL AND R.N. MILLER, *Numerical calculation of stable and unstable periodic solutions to the Hodgkin–Huxley equations*, Math. Biosci, 49 (1980), pp. 27–

- 59.
- [25] J. TOUBOUL, *Nonlinear and stochastic models in neuroscience*, PhD thesis, Ecole Polytechnique, dec 2008.
 - [26] JONATHAN TOUBOUL, *Sensitivity to the cutoff value in the quadratic adaptive integrate-and-fire model*, Research Report 6634, INRIA, aug 2008.
 - [27] JONATHAN TOUBOUL AND ROMAIN BRETTE, *Dynamics and bifurcations of the adaptive exponential integrate-and-fire model*, Biological Cybernetics, 99 (2008), pp. 319–334. PMID: 19011921 DOI: 10.1007/s00422-008-0267-4.